1964

Light absorption, refraction, and scattering in the cavity of a visible helium-neon gas laser

Stuart Armand Schleusener
Iowa State University

LIGHT ABSORPTION, REFRACTION, AND SCATTERING IN THE CAVITY OF A VISIBLE HELIUM-NEON GAS LASER

by

Stuart Armand Schleusener

A Dissertation Submitted to the
Graduate Faculty in Partial Fulfillment of
The Requirements for the Degree of
DOCTOR OF PHILOSOPHY

Major Subject: Electrical Engineering

Approved:

Signature was redacted for privacy.

In Charge of Major Work

Signature was redacted for privacy.

Head of Major Department

Signature was redacted for privacy.

Dean of Graduate College

Iowa State University
Of Science and Technology
Ames, Iowa

1964

TABLE OF CONTENTS

INTRODUCTION

Historical Background

The beginnings of the laser (acronym for "light amplification by stimulated emission of radiation") may be conveniently dated from the time of a theoretical paper by Schawlow and Townes (1) in December, 1958. This paper suggested the possibility of extending the principles of maser action into the infrared and optical regions. The first announcement of success was made July, 1960, by Maiman (2) of the Hughes Aircraft Company whose device used a ruby crystal.

Early in 1961 a helium-neon gas laser at the Bell Telephone Laboratories proved to be operational. A system of this type was first proposed in 1959 by Javan (3) and the subsequent two years of effort by Javan and others proved successful. Additional types of gas lasers have since been discovered which utilize other gases, one type of which is the new gas ion laser utilizing argon, krypton, xenon, and neon. Scientists at Hughes Aircraft Company claim that more than 60 new wavelengths can be obtained ranging down to the ultraviolet, this opening the visible spectrum.

Late in 1962 a new kind of laser was reported in which the coherent light output was produced in the p-n junction of a GaAs semiconductor. Initial announcement of the success of this type of laser was shared by three companies. These companies were the General Electric Company, International Business Machines, and Lincoln Laboratories. In the intervening period a number of other junction lasers have been reported.

The overall progress in discovering new lasing transitions and operating techniques has been explosive. Each month brings new journal reports concerning new discoveries and developments in the laser field. As of this writing, laser power outputs range from a continuous few milliwatts for the gas and junction types to several hundred megawatts and approaching multigigawatts for the pulsed ruby laser with amplifier.

As of this time commercial products representing all three classes (solid-state, gas, junction) of lasers are available. Many groups are active in laser research and development. It is obvious from this progress that the amount of research and development being expended on lasers is considerable. However, only a small percent of this effort has been in the truly applications area. It is in the applications area where extensive research is needed to fully utilize the unique properties of coherent radiation at optical frequencies.

Purpose

Due to the present-day lack of useful laser applications, it was felt that a fruitful area of research would be to try to discover unique laser uses that no other known device could fulfill. To accomplish this it was decided to concentrate effort in doing what shall be called in-cavity experiments with a 6328 angstrom visible-light gas laser. Part of the basis for attempting this work was the existence of a recently constructed gas laser of the above type within the Electrical Engineering department. Cavity accessibility was readily available in this unit.

Light, part of the electromagnetic spectrum, can be refracted,

absorbed, or scattered. In-cavity experiments concerning these three properties of light were attempted in an effort to determine any new practical uses of gas lasers in general.

Physical Description of Laser

The helium-neon gas laser used in the experiments discussed in this dissertation is a device with a continuous output of a few milliwatts of coherent light at a wavelength of 6328 angstroms. Figure 1 is a photograph of the unit in question.

Historically, the first gas lasers were of the Fabry-Perot type using flat multilayer-dielectric internal mirrors. Later, external concave mirrors were also utilized. In the system described here, multilayer-dielectric mirrors of better than 99 percent reflectivity are placed facing one another approximately 120 centimeters apart. A resonant cavity is thereby formed between the two mirrors. This resonant cavity is unique in that there are no side walls as in a microwave cavity. It is this feature that permits the research described in this dissertation to be accomplished.

The gain mechanism for laser operation is due to stimulated emission which is the inverse process of radiative absorption. Because the two mirrors provide a folded path, light beams are reflected back and forth with laser oscillations occurring when the energy gain due to stimulated emission exceeds the energy loss per path traversal. Each mirror provides an escape path of approximately 0.5 percent of the internal beam energy incident on the mirror surface.

Figure 1. Helium-neon gas laser

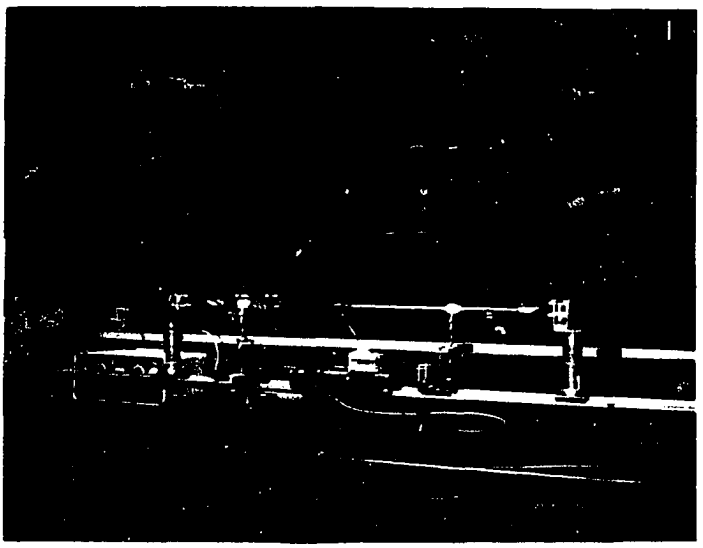

The quartz tube located between the two mirrors contains the helium and neon gas medium where the r-f gas discharge and stimulated emission take place. The quartz tube is about 100 centimeters long thereby leaving a space of about 20 centimeters for in-cavity experiments. The r-f discharge is applied via the center external electrode and the two outer ground paths through the tube clamps. At each end of the tube is an optical flat inclined at the Brewster angle with respect to the incident light beams. Brewster angle inclination minimizes reflection losses for axially-directed radiation polarized in the plane of incidence. Reflection losses for light polarized normal to the plane of incidence are not similarly minimized. Since all other factors in the system are essentially the same for the two beam polarizations, the laser output is polarized in the plane of incidence as determined by the spatial orientation of the optical flats.

Bennett (4) states that the gain of a 6328 angstrom helium-neon gas laser is about two per cent per meter of discharge tube length for a discharge tube diameter of seven millimeters. Since the gain is inversely proportional to the diameter, the two percent figure is not unique for all 6328 angstrom gas lasers. However, the laser used in these experiments has a six millimeter diameter tube and so can be expected to have a gain in the two percent range. Due to such low gain it was dubious as to just what work could be done in the cavity without introducing too much loss and thereby quenching oscillations. Also, the boundaries of any experimental setup within the cavity would of necessity have to consist of optical flats placed at the Brewster angle.

Therefore, the primary prerequisite before anything could be accomplished was to find out whether two optical flats could be inserted without they themselves causing quenching.

Three optical flats were purchased from the American Optical Company of Plainfield, New Jersey for use in the proposed in-cavity work. These optical flats were flat to within 1/10 wavelength and were made from three millimeter thick pyrex.

Laser output dropped considerably when the first flat was inserted into the cavity. However, part of the decrease in output was due to the extra transverse beam displacement caused by the added glass path length resulting in cavity misalignment. Realignment raised the output appreciably, but of course not to the previous level attained without the added flat.

Inserting the second flat gave rise to the same problems as the first with the end result of satisfactory lasing operation being attained, although at a substantially reduced level. Therefore, it was proven that a test cell could be inserted into the cavity for experimental uses.

REFRACTION

At this point in the project, much thought was given to the feasibility of using an in-cavity absorption cell as a very sensitive detector of possibly oxygen or ozone. To this end, a twelve-inch absorption cell was constructed for insertion into the cavity with the cavity operating in a non-confocal configuration due to increased mirror spacing. Since oxygen is slightly absorbent at a wavelength of 6328 angstroms, it was felt that removing the air, consisting of about twenty percent oxygen, from the cell would possibly result in a quite noticeable increase in lasing intensity. The actual observed result was about a fifty percent decrease in output when a vacuum was applied to the test cell.

The amount of decrease seemed to depend on the alignment of the cavity. This indicated that the change of the index of refraction of vacuum compared to air at atmospheric pressure was enough to detune the cavity through the change in the twelve-inch test cell. Figure 2 illustrates the test setup for observing effects of changes in the index of refraction within the cavity.

The index of refraction of air relative to a vacuum and for a temperature of zero degrees centigrade and 760 millimeters of mercury pressure is 1.0002926 at the sodium D wavelength. For other than these standard conditions, it is possible to obtain the index of refraction of a medium by using equation 1 relating index of refraction and density

$$\frac{n^2 - 1}{(n^2+2)\rho} = \text{constant} \qquad 1$$

where n is the index of refraction and ρ is the density. Equation 1 is

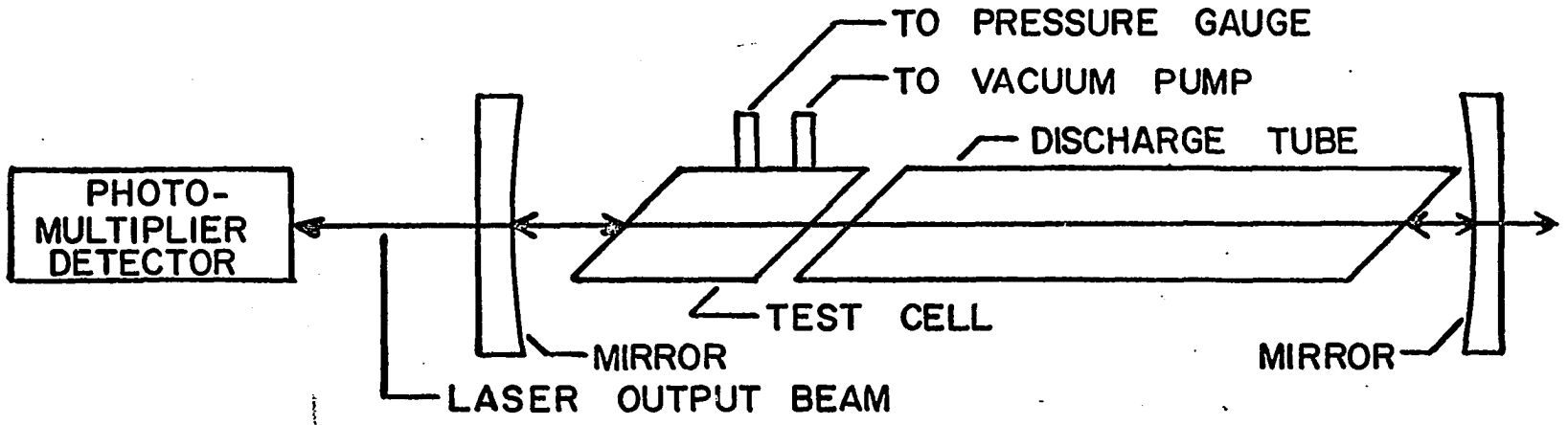

Figure 2. Index of refraction test system

called the Lorentz-Lorenz formula and relates the macroscopic-optical properties of a medium to the number and properties of the particles. For gases, equation 1 can be simplified by noting that as for air, the index of refraction very nearly equals one and that $n + 1 \approx 2$ and $n^2 + 2 \approx 3$. This gives

$$\frac{n^2 - 1}{(n^2 + 2)\rho} = \frac{(n + 1)(n - 1)}{(n^2 + 2)\rho} = \frac{(n - 1)2}{3\rho} \qquad 2$$

Thus, for gases it may be written

$$\frac{n - 1}{\rho} = \text{constant} \qquad 3$$

This equation is the Gladstone-Dale relationship and is based on the assumption that refraction is a molecular process with the amount of refraction being proportional to the number of molecules present.

Since the change in laser output, due to removing air from the test cell, is so substantial, it was decided to try to enhance this effect and report the resulting sensitivity that could reasonably be obtained.

It was then observed that the presence of a slit on the photomultiplier face further enhanced the output changes providing that the beam was placed on the proper edge of the slit. Were it not, the output change caused by transverse beam movement would work against the output change caused by cavity misalignment resulting in small test cell effects. In other words if the beam movement on the slit edge is such as to increase photomultiplier output, then the cavity should be detuned to the point where the change in test cell air density tends to increase output by improving cavity alignment. The same sensitivity could also be achieved by using these two effects together in a negative

sense.

Since the output beam displacement effect is quite noticeable, it seemed possible that the one plane-one spherical mirror configuration would be perhaps more sensitive than the concave-concave configuration that was first used. The reasoning behind this is that the output beam from the end of the cavity with the plane mirror has a very small cross-section. Therefore, any transverse displacement on the slit edge would increase the output change due to beam movement. To use the plane-spherical mirror configuration, it was necessary to build a three-inch test cell, the twelve-inch cell being too long. The plane-spherical system demands very nearly mirror spacing of 120 centimeters for oscillations to occur only leaving about 12 centimeters for test cell space.

Figure 3 shows how the output changes when the pressure of the three-inch test cell was varied. Note that the combination of cavity misalignment and transverse movement of the output beam results in a sensitivity of about 15 millivolts per millimeter of mercury from the low millimeter to about 300 millimeter range. This sensitivity cannot necessarily be held to for one run over all pressure ranges but appropriate system detuning near the middle of a desired range can centralize the effect where needed.

It is not at all obvious as to just why there should be any useful output beam displacements resulting from removing or replacing air in a cavity test cell. Figure 4 helps explain not only the displacement effect but also the cause of cavity alignment changes.

Figure 4 was constructed by starting at point G and using the law

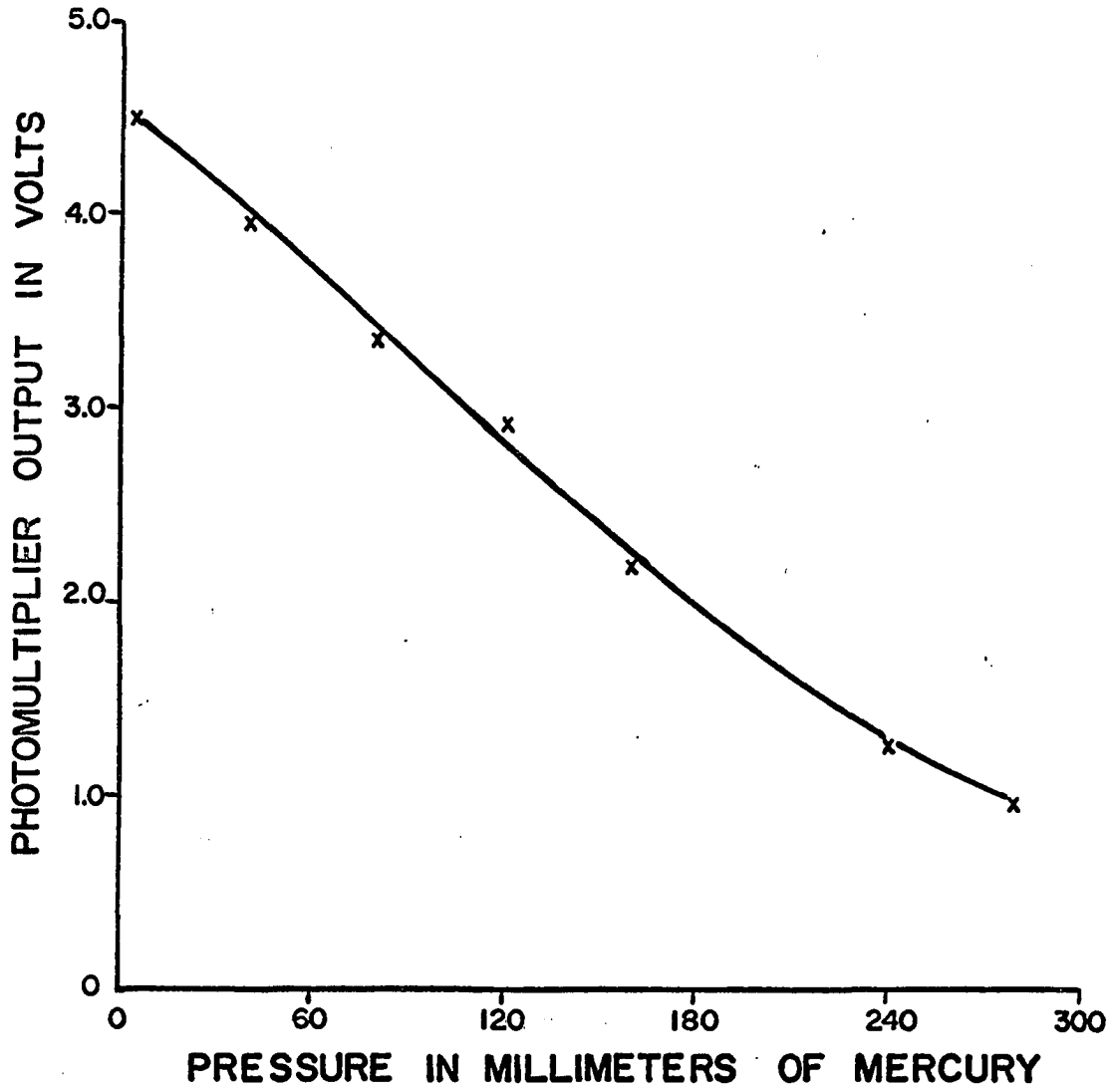

Figure 3. Effects of changing the index of refraction

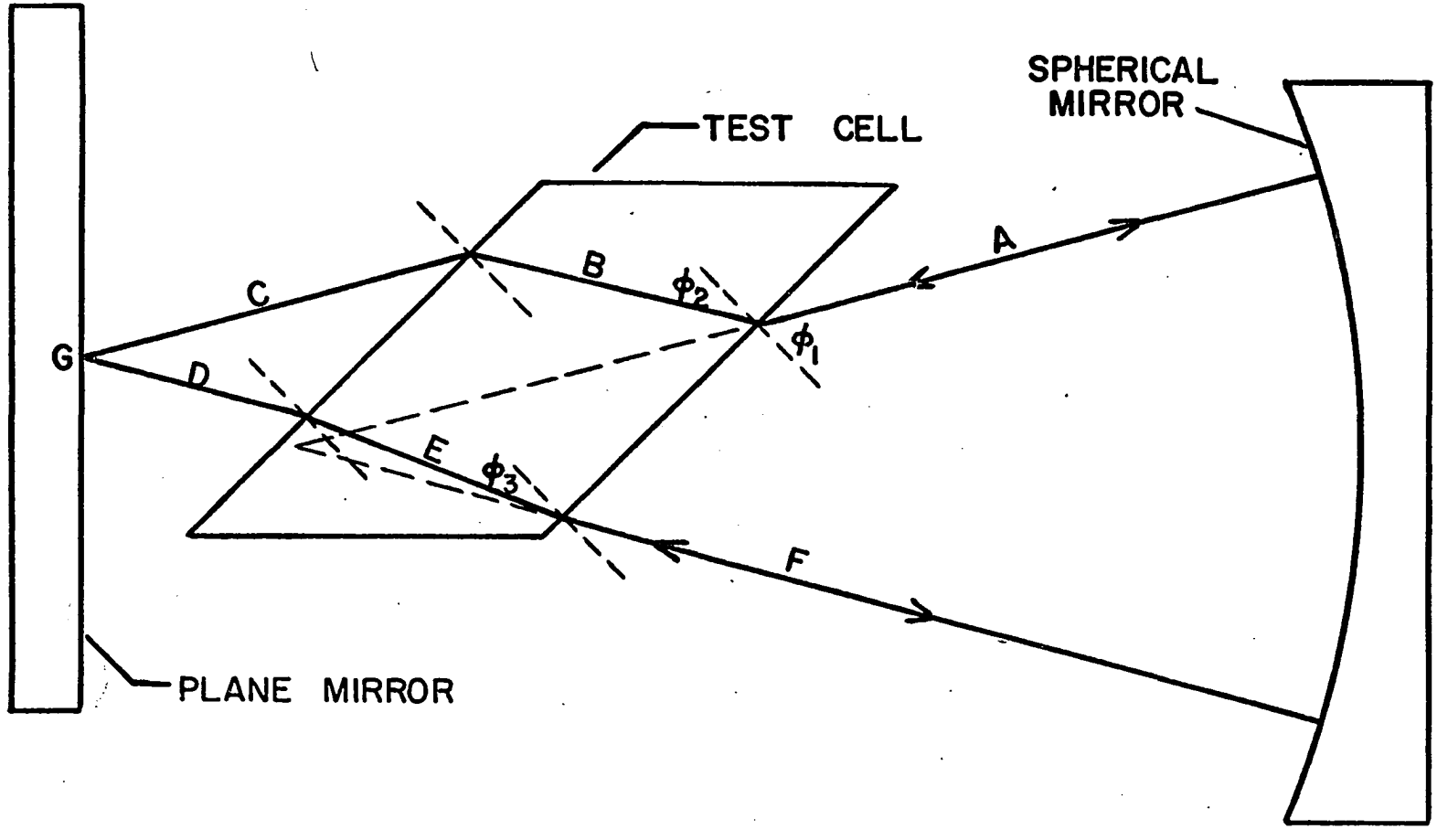

Figure 4. Index of refraction test cell with ray deviations

of reflection to construct rays C and D. The law of reflection states that the angle of incidence equals the angle of reflection. Rays B, A, E, and F were constructed using Snell's law of refraction

$$n_1(\sin\phi_1) = n_2(\sin\phi_2) \qquad 4$$

where n_1 is the index of refraction of the incident medium, n_2 the index of refraction of the transmitted medium, ϕ_1 the angle of incidence, and ϕ_2 the angle of refraction. An interesting feature of Figure 4 is that the apparent radius of curvature of the spherical mirror does not seem to occur on the face of the plane mirror. The Brewster-angled test cell is not cylindrically symmetrical and therefore is the cause of the apex displacement from the plane mirror face.

It is necessary to examine the situation that exists when the air density in the test cell is reduced, thereby reducing its index of refraction according to the Gladstone-Dale law, equation 3. From Snell's law it is apparent that reducing n_2 increases ϕ_2 because

$$\phi_2 = \sin^{-1}\frac{(n_1\sin\phi_1)}{n_2} \qquad 5$$

It is best to start at the spherical mirror with rays A and F which lie on a radius of curvature chord of the present spherical mirror position. It will be these rays that have the highest gain since they will make more passes before being lost out of the cavity. The angle of refraction, ϕ_2 and ϕ_3 of rays A and F respectively, will be greater as discussed above; thus, both B and E will be lowered thereby lowering their contact points with the plane mirror surface. This effectively lowers the output beam and causes the output beam displacement. Note, that these two points will no longer be one and the same because the increase in

ϕ_2 will be more than the increase in ϕ_3 due to the greater angle of incidence. Therefore, cavity misalignment occurs.

To maximize the sensitivity it is necessary to determine the answers to two questions; namely, what the best distance of the slit from the mirror is and what the best position of the slit in the beam cross-section is. Since the output beam has a circular cross-section it is apparent that the maximum change of energy into the photomultiplier per transverse displacement change occurs when the straight edge is on a diameter perpendicular to the movement. That there isn't any best distance from the mirror is readily ascertained by noting that the increase in transverse motion experienced at greater distances from the cavity leads to an increase in sensitivity that is cancelled by the decrease in sensitivity caused by the increase in beam cross-section.

In conclusion, it seems that the cavity of a gas laser can be effectively used to measure changes of index of refraction. These changes appear to be measured with more sensitivity due to the extra effect of cavity misalignment. The time response of these changes will be limited only by the photomultiplier detector which can be made to respond in the nanosecond region.

VARIABLE BREWSTER-ANGLE FLAT

Laser Energy Levels

To accomplish any low-loss in-cavity experiments it is desirable to have an in-cavity loss calibration device. Some understanding of the laser gain mechanism is necessary in order to understand the effects of using such a device.

The only general requirement for a laser system is that it provide an upper energy state into which atoms can be pumped and a lower state to which they will return with the spontaneous emission of photons. The system must also allow a population inversion between the two states. The noble gas neon meets both of the above requirements and as such is the medium in which stimulated emission takes place in the helium-neon gas laser.

Fundamental to an understanding of the operation of a laser is an understanding of stimulated emission. To illustrate stimulated emission consider a neon atom in the ground state in Figure 5. If left unperturbed by any outside influence, it will remain in the ground state indefinitely. However, if the atom is placed in an electromagnetic field, it may absorb a photon from the field and subsequently be found in an upper, say 3S for example, excited energy state. The atom has thus been induced or stimulated to make a transition from the lower of two energy states to an upper excited energy state. After the transition has been made, the energy of the atom has increased by $E = hf = E_{3S} - E_g$ where h is Planck's constant and f is the frequency of the stimulating

Figure 5. Energy level diagram for a helium-neon gas laser

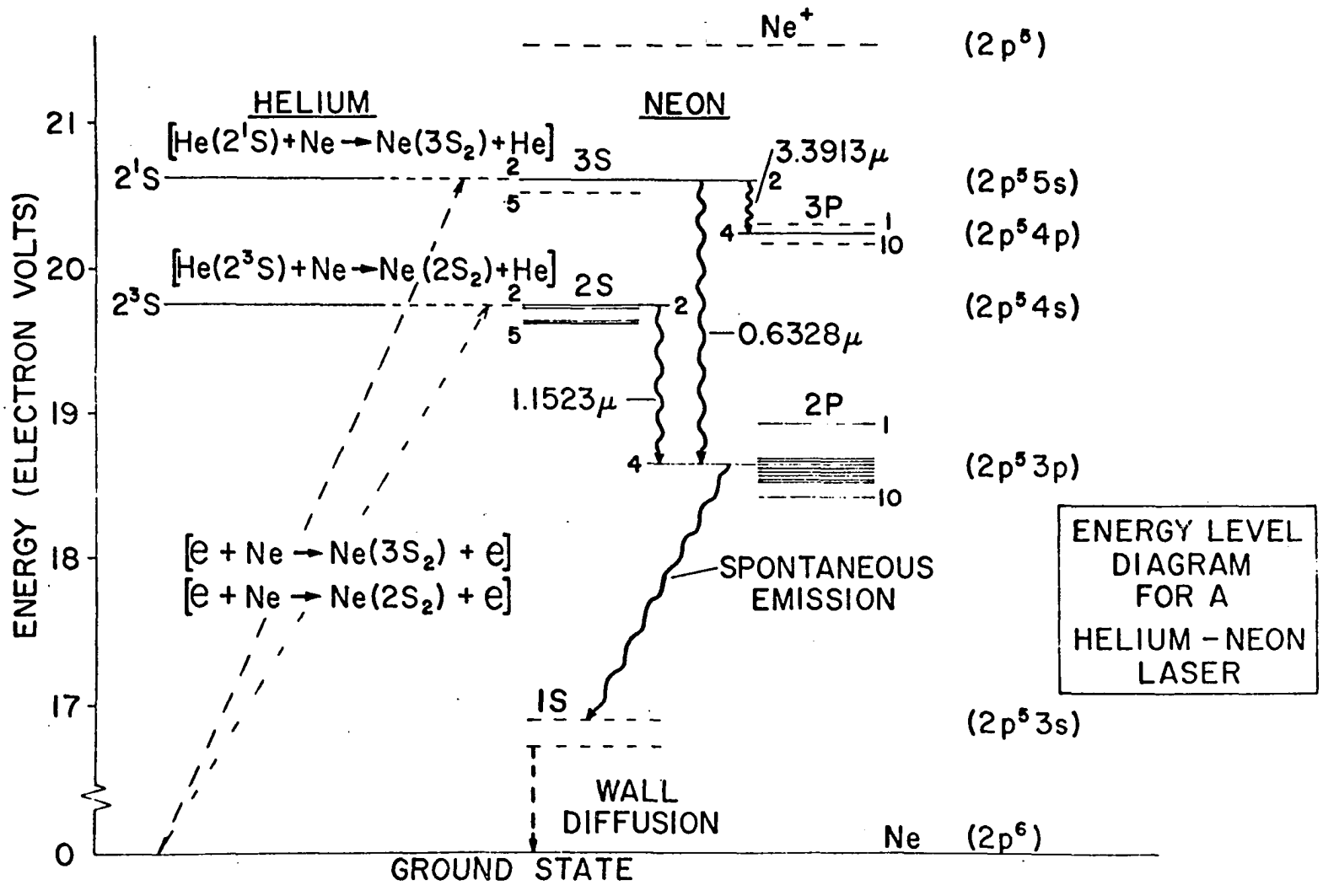
Ne+
(2p5)
HELIUM
NEON
21
[He(2'S)+Ne→Ne(3S2)+He]
2'S
3S
2
5
3.3913μ
2
3P
4
1
10
(2p5 5s)
(2p5 4p)
20
[He(2³S)+Ne→Ne(2S2)+He]
2³S
2S
2
5
2
(2p5 4s)
0.6328μ
1.1523μ
19
2P
1
4
10
(2p5 3p)
18
[e + Ne → Ne(3S2) + e]
[e + Ne → Ne(2S2) + e]
SPONTANEOUS EMISSION
ENERGY LEVEL DIAGRAM FOR A HELIUM – NEON LASER
17
1S
(2p5 3s)
WALL DIFFUSION
0
Ne
(2p6)
GROUND STATE
ENERGY (ELECTRON VOLTS)

photon. Following a transition, the energy in the electromagnetic field will have decreased by an amount equal to the increase in the energy of the atom. This particular phenomenon is well known and is called absorption.

In a way which is completely analogous to absorption, an atom initially in its excited state, again say 3S for example, may interact with photons having the energy E and be induced to make a transition to its ground state. The probabilities that transitions from either the ground to an excited state or the same excited state to the ground state will occur are the same. A very important difference between the two, however, is that in absorption a photon is destroyed and the atom acquires its energy, whereas in stimulated emission a photon is created and the atom loses energy. Therefore, if one could prepare a number of atoms in their excited states and allow them to interact with photons each having an energy E, they could be stimulated to emit more photons of energy E, thus increasing the overall intensity of the radiation field. If one can continuously maintain more atoms in the excited state than in the ground state, one may thereby amplify radiation of a frequency $f = E/h$.

Stimulated emission has the same phase, propagation direction, and polarization plane as the stimulating photon. The similarity between the stimulated emission and initiating photon is complete and is the basic mechanism of laser action.

Laser Gain

As mentioned before, the gain of a 6328 angstrom helium-neon gas laser is about two percent per meter. Therefore, one would expect a gain of about two percent for the laser used herein. Later, in this dissertation, this gain figure is experimentally verified.

The gain of a gas laser operating at saturation (peak output) conditions is less than that at lasing cutoff (no oscillations) for the same degree of excitation of the gaseous media. This is because at saturation, many photons are involved and are stimulating many excited atoms to radiate thereby decreasing the population inversion and leaving fewer excited atoms available for stimulation by following photons. At or near cutoff, under the same discharge conditions, any photon will find more excited atoms available for stimulation, resulting in a higher gain.

From the above, it is apparent that any method of cavity loss calibration which was attempted exterior to the cavity would be beset with difficulties. Factors complicating such an analysis would be lack of a linear detector in addition to the more difficult problem of not knowing what the gain changes to at various loss levels.

In-Cavity Calibration

One way of overcoming the loss calibration difficulty would be to have a known variable loss element in the cavity. Then, the calibrating loss could be varied until the output was the same as when the test specimen was inserted. Removal of the test material must not change the index of refraction appreciably because this would disturb the output

and give rise to errors. It is because of this that this type of procedure is limited to testing gas vapors for absorption or aerosols for light scattering along with the necessity for testing only those substances with low losses. The low-loss criterion is really the major advantage of this type of measurement in that very low losses of light can be detected in this fashion.

A possible way of providing a known variable loss is to use an adjustable-angle optical flat. The losses at both the air-to-glass and glass-to-air surfaces are well known so that for any angle, the losses due to reflection can be calculated. Losses due to scattering inside the flat itself can be considered constant. The only obvious difficulty is the transverse beam displacement caused by changing the angle of such a calibrating flat. This displacement can be minimized by having the variable Brewster-angle flat (VBAF) be as thin as possible.

Before purchasing such a piece of glass it was necessary to determine about how much transverse displacement could be tolerated without misaligning the cavity. The aforementioned twelve-inch test cell had characteristics such that when the system was deliberately misaligned, the output changed substantially. However, when the system alignment was peaked, removal of the air made very little difference on the output. Therefore, if VBAF beam displacement was less than that caused by an air-to-vacuum change in the twelve-inch cell; then, one could expect only small errors when calibrating. It was determined that removing the air in the twelve-inch cell resulted in a transverse displacement change of about five-thousandths of an inch (five mils). This was the allowable

limit set on transverse displacement changes caused by varying the VBAF angle.

The next step is to determine how many degrees variation from the Brewster-angle are necessary to create a two percent loss. The cavity beam is polarized in the plane of incidence at the discharge tube ends and proposed VBAF surfaces. Born and Wolf (5) give the equation

$$R_{11} = \frac{\tan^2(\phi_i - \phi_t)}{\tan^2(\phi_i + \phi_t)} \qquad 6$$

as the loss due to reflection at a boundary between two dielectrics. The proportion of the reflected energy to the incident is R_{11}. The angle of incidence is ϕ_i while ϕ_t is the refracted angle. When $\phi_i + \phi_t$ approaches $\pi/2$, the denominator of equation 6 approaches infinity making R_{11} approach zero. Using this fact in conjunction with Snell's law,

$$n_i(\sin\phi_i) = n_t(\sin\phi_t) \qquad 7$$

it can be shown that

$$\sin\phi_t = \sin\left(\frac{\pi}{2} - \phi_i\right) = \cos\phi_i \qquad 8$$

$$\tan\phi_i = n \qquad 9$$

where $n = n_t/n_i$, the index of refraction for refraction from the first into the second medium. Pyrex has a refractive index of about 1.48 compared to air. Therefore, for n = 1.48, the Brewster-angle for an air-pyrex boundary is $\phi_i = \phi_B = 56$ degrees.

Snell's law, equation 7, relates the refracted angle to the angle of incidence. Using equation 6 together with equation 7, a table of

values of total loss for both boundaries of the VBAF may be calculated. Table 1 lists the values of a computer run with ϕ_i varying from 56 to 66 degrees. For the two percent attenuation that was needed, examination of Table 1 reveals that $\phi_i = 64$ degrees.

Table 1. Variable Brewster-angle flat (VBAF) loss versus angle

ϕ_i	ϕ_t	Loss
56.0	34.067	0.0000004
56.5	34.294	0.0000640
57.0	34.518	0.0002406
57.5	34.740	0.0005387
58.0	34.960	0.0009670
58.5	35.177	0.0015350
59.0	35.392	0.0022524
59.5	35.604	0.0031297
60.0	35.814	0.0041780
60.5	36.021	0.0054091
61.0	36.225	0.0068353
61.5	36.427	0.0084696
62.0	36.626	0.0103259
62.5	36.822	0.0124188
63.0	37.016	0.0147637
63.5	37.206	0.0173768
64.0	37.394	0.0202753
64.5	37.579	0.0234772
65.0	37.761	0.0270014
65.5	37.940	0.0308680
66.0	38.116	0.0350980

It is necessary to determine the change in transverse displacement from $\phi_i = 56$ degrees to $\phi_i = 64$ degrees. Figure 6 illustrates the ray geometry followed by light incident at an angle ϕ_i. The difference in y for $\phi_i = 56$ and 64 degrees is the change in transverse displacement that we need to calculate. For $\phi_i = 56$ degrees, $\phi_t = 34$ degrees and

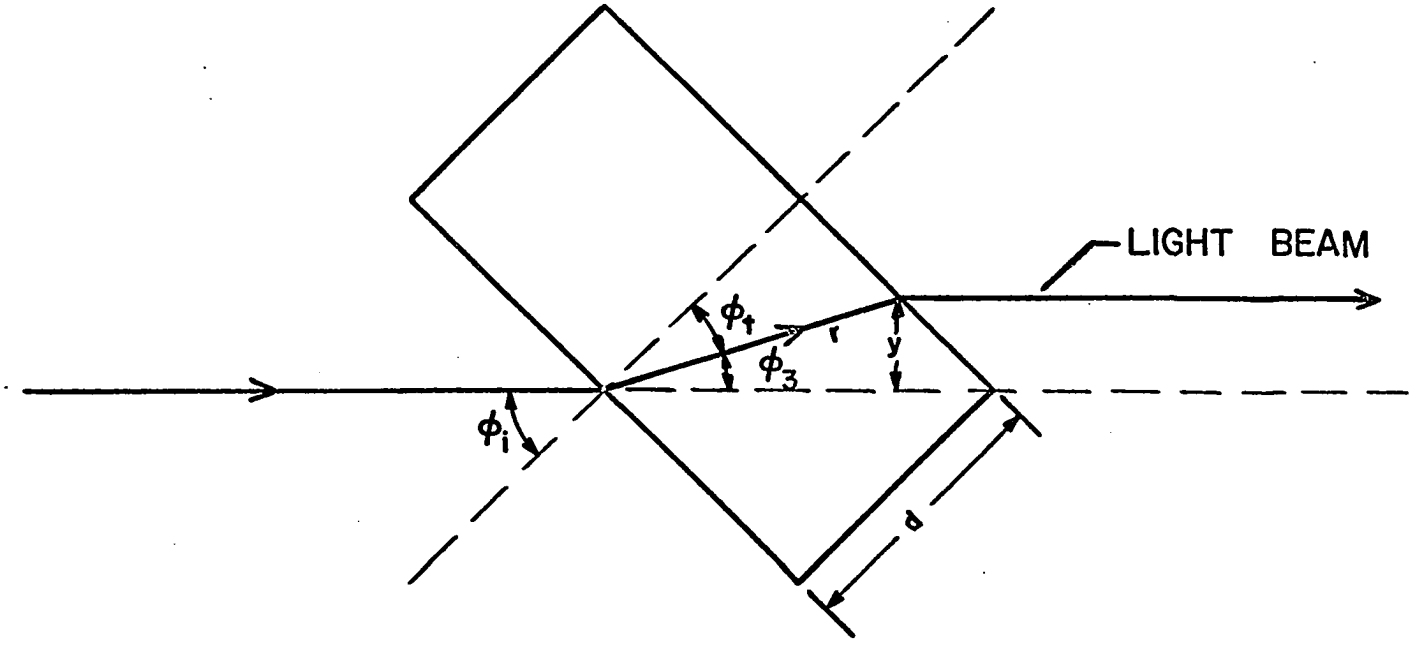

Figure 6. Variable Brewster-angle flat

$$d = r(\cos 34^{\circ}) \tag{10}$$

$$r = 1.2062d \tag{11}$$

$$\phi_3 = 22^{\circ} \tag{12}$$

$$y = r(\sin\phi_3) \tag{13}$$

$$= (1.2062d)(0.37461) \tag{14}$$

$$= 0.452d \tag{15}$$

Similarly, for $\phi_1 = 64$ degrees,

$$y = 0.562d \tag{16}$$

Subtracting the two displacements gives the change as 0.11d where d is the flat thickness. Knowing that about 5 mils change can be tolerated, it is possible to set

$$0.11d = 5(10^{-3}) \text{ inches} \tag{17}$$

$$d = 1.15 \text{ millimeters} \tag{18}$$

Therefore, a VBAF of about one millimeter thickness will not cause too much cavity misalignment for an angle change of 56 to 64 degrees.

The actual purchased VBAF was flat to 1/10 wavelength and had a thickness of 18 mils. From the above considerations, transverse beam displacement effects should be negligible over the desired angle range.

The thinness of the VBAF seemed to present a problem in that it appeared that the reflections from the glass-to-air boundary could change the boundary conditions at the air-to-glass boundary. Such an effect might invalidate equation 6 which is used to calibrate the VBAF with respect to angular variations. To check this possibility several test runs were made, one using the 18 mil flat; the other using a three millimeter flat. At the angles involved the thickness of the three milli-

meter flat was sufficient to provide separate beam reflections from both boundaries. Therefore, this flat should cause no boundary interference effects. Figure 7 illustrates the comparison between the 18 mil and three millimeter flats. The compared tests were run with angles of incidence less than usual so that the boundary interference effect would be more pronounced and cavity misalignment caused by the thicker flat would be minimized. The curves coincide quite well indicating that the supposed boundary interference effect of the 18 mil VBAF can be neglected.

To determine the sensitivity of the cavity to losses, it is first necessary to calibrate the photomultiplier to remove its characteristic effects from the laser output measurements. Figure 8 shows the resulting curve obtained by calibration with neutral density filters. Then, by varying the VBAF angle, data was obtained for Figures 9, 10, and 11. Figure 9 shows how laser output varies for various VBAF angles. Figure 10 illustrates the relationship between laser output and cavity losses. Note in Figure 11 that a one-hundredth of one percent loss change is readily detectable because it results in a photomultiplier output change in the order of 50 millivolts. Therefore, ultimate sensitivity is better than one part in ten thousand for detecting incident light losses per pass at a wavelength of 6328 angstroms. Flattening out of the end of the curve in Figure 11 indicates a decrease in sensitivity and provides a desirable range increasing effect.

In conclusion, modification of the laser cavity by inserting a thin variable-angle flat and a test cell transforms the laser into a useful low-loss light detector. This low-loss light detector operates at one wavelength only and has an ultimate sensitivity of about one part in ten

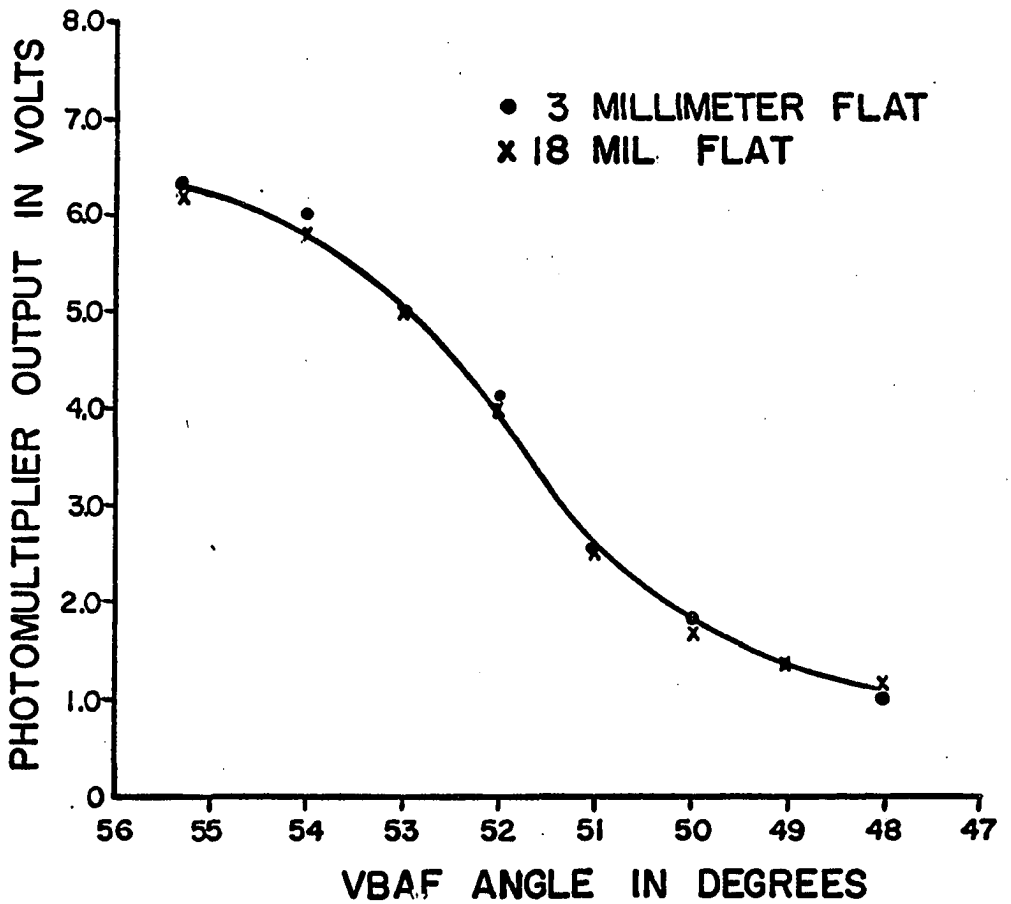

Figure 7. Variable-angle flat comparison

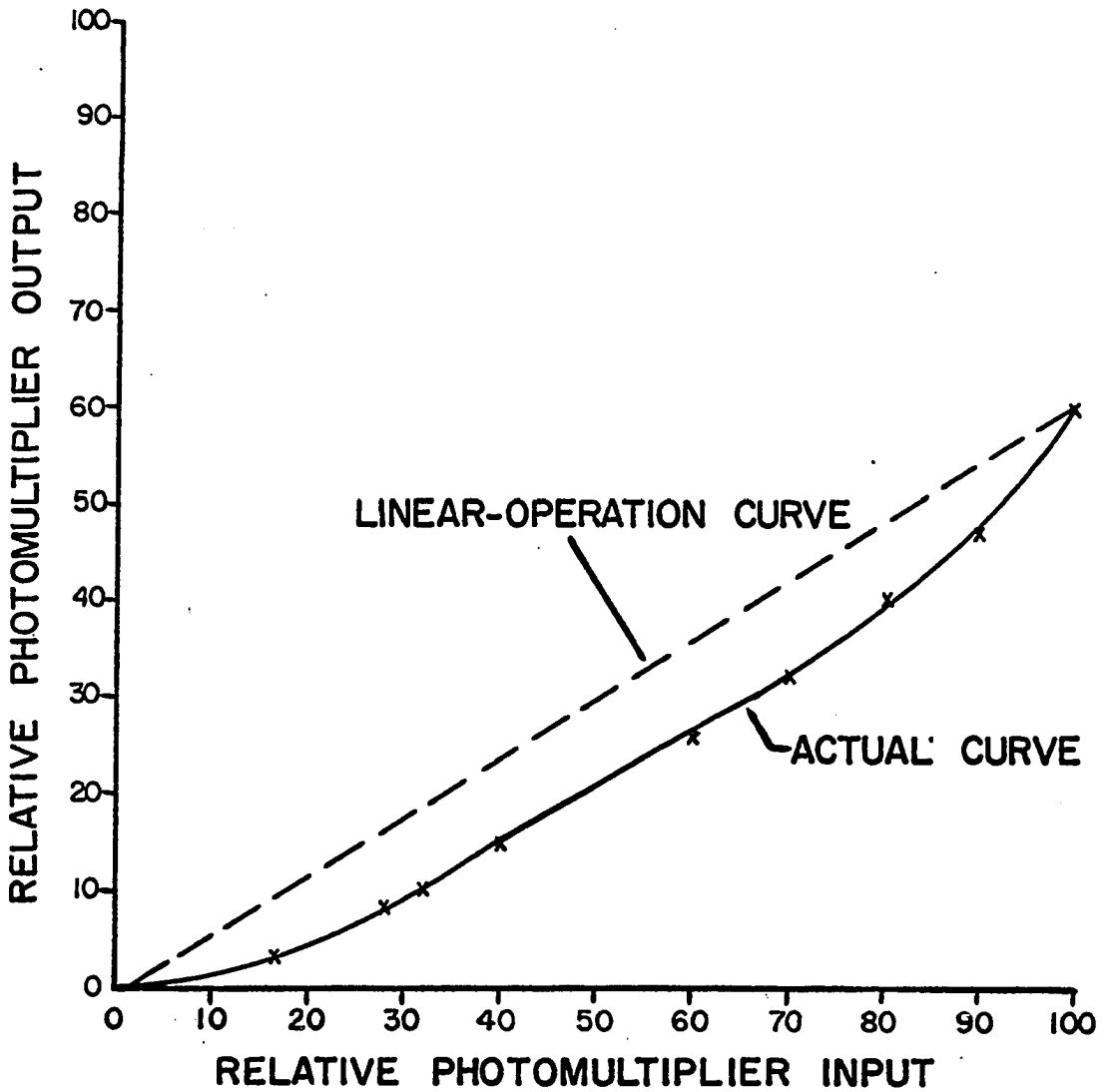

Figure 8. RCA type 7102 photomultiplier calibration curve

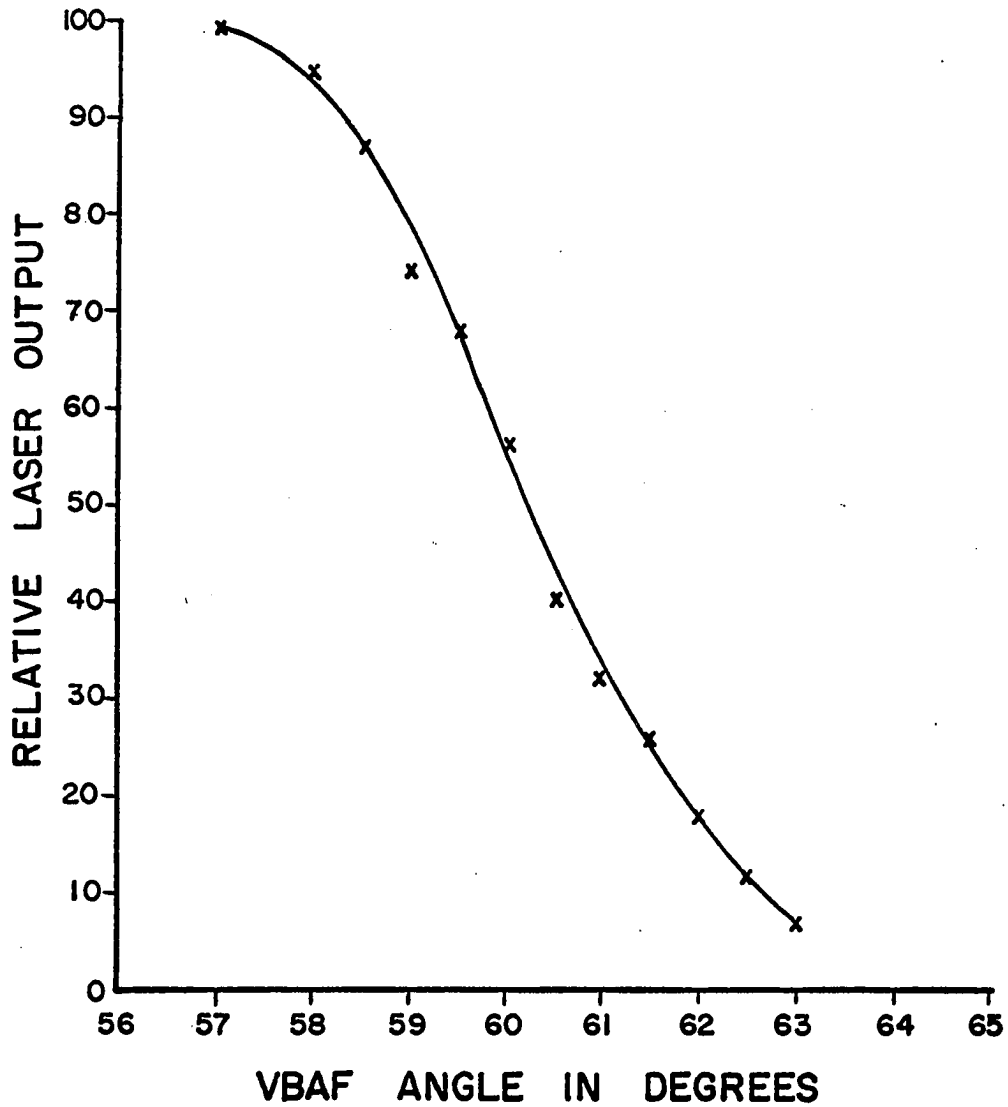

Figure 9. Laser output power versus VBAF angle

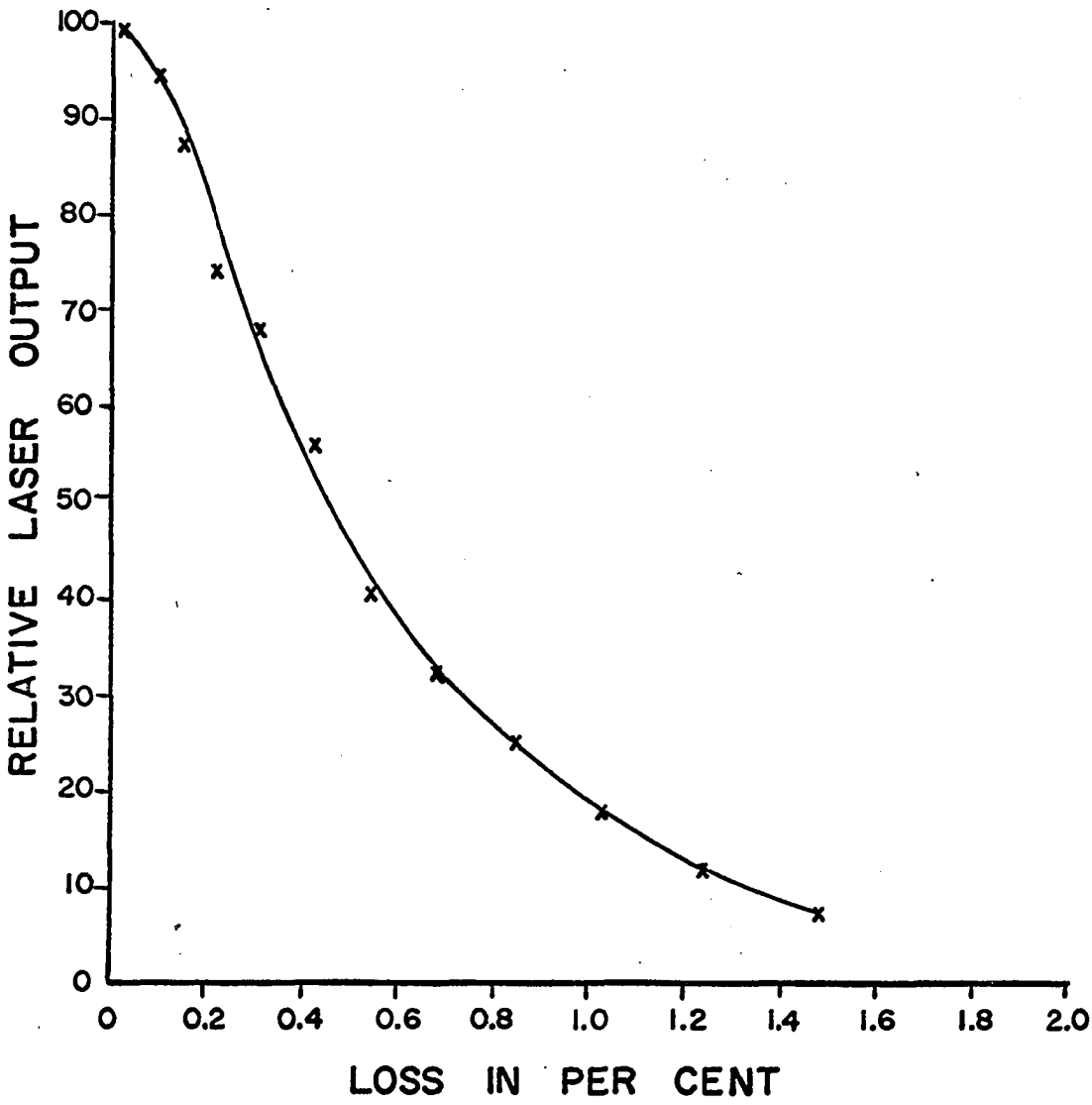

Figure 10. Laser output power versus cavity losses

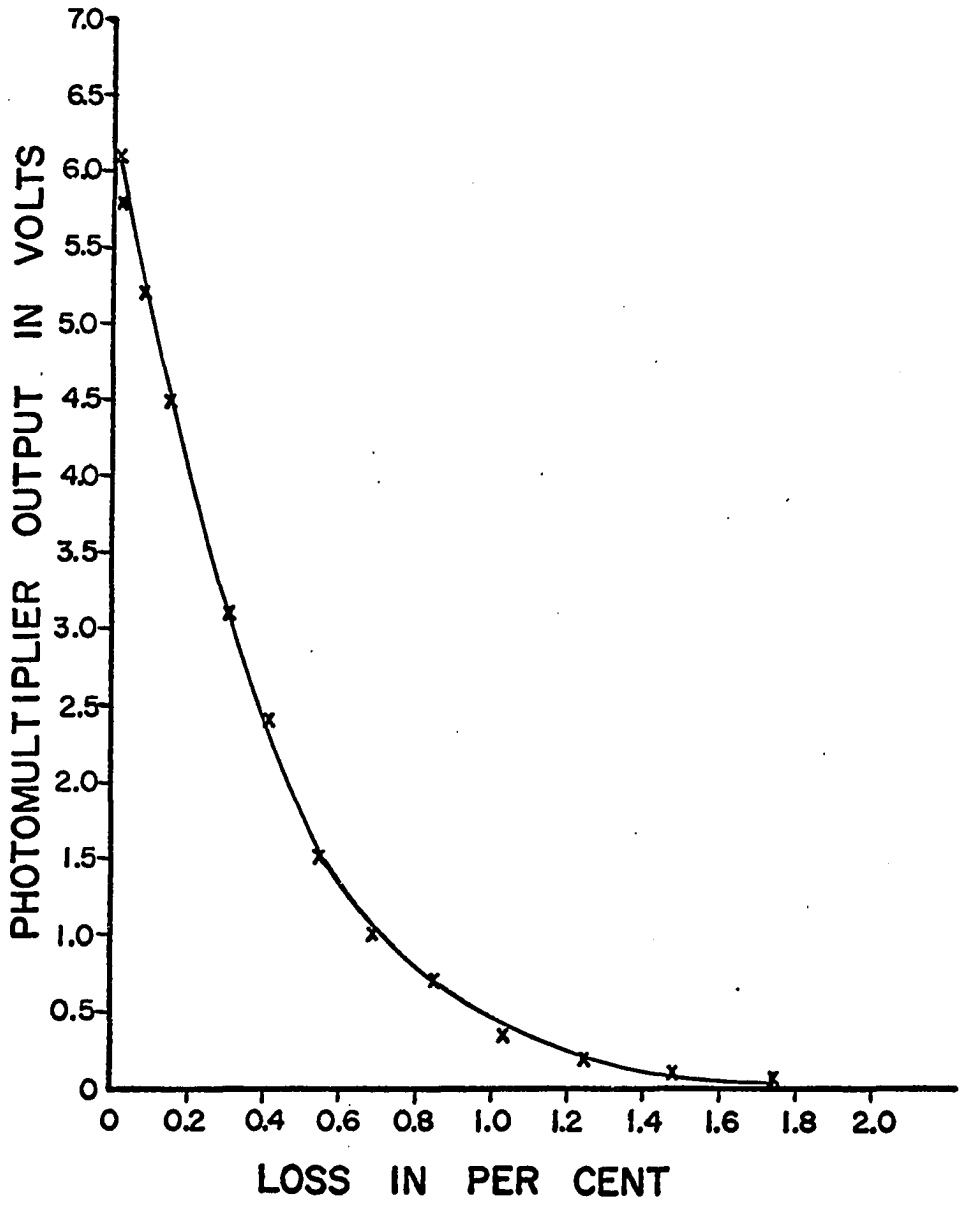

Figure 11. Photomultiplier output versus cavity losses

thousand and a loss range of about one percent. Use at other wavelengths necessitates using other gas lasers.

ABSORPTION

When light or any other form of electromagnetic radiation passes into a transparent medium, it can interact with it in three ways; it can be reflected at the surfaces, scattered in the medium, or absorbed. The cavity test cell and test components are limited in position and type such that reflection losses are minimized. Scattered light tests are considered in full in the next section. Absorption work at a single wavelength is limited in scope and is presented primarily to demonstrate the high sensitivity of the system.

Lothian (6) states that the transfer of an atom or molecule from the ground state to higher states can be effected by the absorption of radiation. For every transfer there is a corresponding absorption of a quantum of radiation of appropriate frequency. Hence, if radiation of a continuous range of frequencies is incident on the vapor of a monatomic element, a series of absorption lines corresponding to transfers from the ground state will be observed. The lines of the so-called principal series appear because the incident radiation normally finds all the atoms in their ground state. Under certain conditions, however, some of the atoms may be found in excited states and absorption lines corresponding to these states as initial states will be observed.

The absorption spectra of molecules are much more complicated and consist not of lines but of groups of bands (spectral regions over which a whole range of wavelengths is apparently absorbed). The energy of a molecule is made up of three parts, that of its electrons, that associated with vibrations within the molecule, and the energy of rotation.

Each of these energies is quantized just as the electronic energy of an individual atom is quantized. The molecule can thus exist only in a limited number of electronic, vibrational, and rotational states. The absorption bands in the far infrared correspond to transitions from one such rotational state to another, and their long wavelength indicates that the energy changes involved are very small, about one-hundredth of an electron-volt or less. A transition of the molecule from one vibrational state to another may be accompanied by a simultaneous rotational transition, which may differ from molecule to molecule even though they are all undergoing the same vibrational change. The absorption spectrum that results does not, therefore, consist of a single line but of a number of closely spaced lines separated by amounts corresponding to the very small differences in the energies of the rotational states. It is these lines that constitute the fine structure of the vibration-rotation bands. Since, energy-wise, 6328 angstroms lies in a region corresponding to the vibration-rotation bands, the electronic band structure (which requires more energy) will not be considered.

Quantitative measurements of absorption are based on two fundamental laws concerning the relationship between the intensities of the radiation on and transmitted by a layer of absorbing substance. The first of these is Lambert's law, which states that the amount of light absorbed by a transparent medium is independent of the intensity of the incident light and that each successive unit layer of the medium absorbs an equal fraction of the light passing through it. Mathematically, Lambert's law is given by

$$I = I_0 e^{-al} \qquad 19$$

where I_o = intensity of the incident light, I = intensity of the transmitted light, l = thickness of the layer, and a = the absorption coefficient of the medium. It is apparent that the absorption coefficient a does not contain any concentration factor. The other important law, Beer's law, deals with this concentration variable. It states that the light absorption is proportional to the number of molecules of absorbing substance through which the light passes. Mathematically, Beer's law is given by

$$I = I_o e^{-kcl} \qquad 20$$

where the new parameters k and c are the extinction coefficient and the concentration variable respectively. The numerical value of k obviously depends on the units of concentration and length.

The output of a gas laser consists of a number of discrete frequencies contained in a doppler band of about 1200 megacycles. It is apparent that an absorption test using such fixed frequencies is of necessity a hit or miss proposition unless conducted on a specimen with broad bands. To check the calibration and sensitivity of a VBAF-laser system, it was decided to measure the absorption of iodine vapor at a wavelength of 6328 angstroms. Iodine vapor exists as a diatomic gas, I_2, with the corresponding vibration-rotation bands. Figure 12 illustrates the test setup.

Goy and Pritchard (7) measured the absorption of iodine in the visible band. They used conventional methods and a test cell of five centimeter length in the presence of an atmosphere of air at 51 degrees centigrade. Near 6328 angstroms they measured an absorption of about

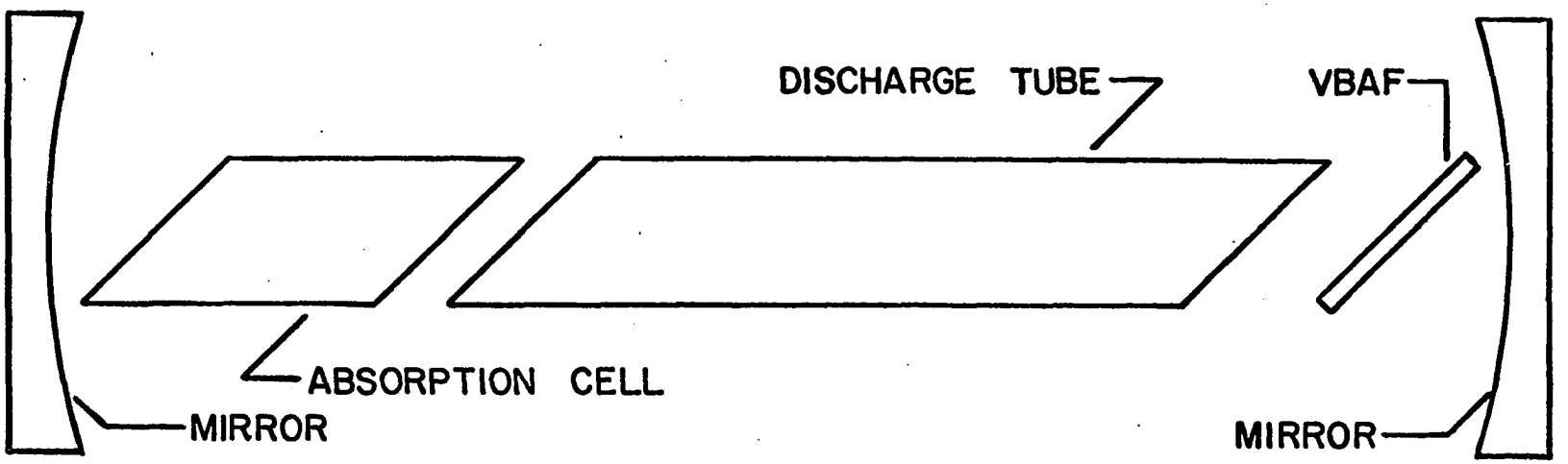

Figure 12. VBAF-laser absorption measuring system

12 percent for their particular test cell.

Several test cells were constructed for insertion into the laser cavity, but each proved too long in that laser oscillations were completely quenched. Finally, a cell with a path length of one-half inch was tried and proved successful. For this one-half inch cell, laser output dropped to near extinguishment. The corresponding position of the VBAF for the same output turned out to be 60.5 degrees. The loss associated with this angle is 0.54 percent which, therefore, is the measured loss of the I_2 vapor in the half-inch cell.

To check the above result against that of Goy and Pritchard (7) it is necessary to use equation 21 representing the vapor pressure of solid iodine as

$$\log P_{atm} = \frac{-3512.8}{T} - 2.013 \log T + 13.374 \qquad 21$$

Equation 21 gives the pressure of the referenced literature test at 51 degrees centigrade as 2.43 millimeters of mercury and the laser absorption test at room temperature as 0.39 millimeters of mercury. Then, using the perfect gas law, one can obtain the relative number of molecules in the two tests as

$$c_{27} = 0.173 c_{51} \qquad 22$$

Using Beer's law, percent loss can be represented by

$$\% \text{ loss} = (1 - e^{-kcl})(100) \qquad 23$$

Substituting the twelve percent loss figure into equation 23, it is possible to solve for kc_{51}.

$$kc_{51} = 2.56(10^{-2}) \qquad 24$$

Now

$$kc_{27}l = k(0.173c_{51})l = 4.44(10^{-3})l \qquad 25$$

Substituting the length of the test cell as 1.27 centimeters

$$kc_{27}l = 5.64(10^{-3}) \qquad 26$$

To calculate what the loss of the test cell should be from the referenced literature test, the value of equation 26 is substituted into

$$\% \text{ loss} = (1 - e^{-kcl})(100) \qquad 27$$

$$= (1 - e^{-5.64(10^{-3})})(100) \qquad 28$$

$$= (1 - 0.9944)(100) \qquad 29$$

$$= 0.56 \qquad 30$$

Note the amazingly close comparison between the actually measured value of 0.54 percent and the referenced literature value of 0.56 percent.

What was wanted in the above test was not so much exact comparison with someone else's results, as the demonstration of the test sensitivity. Compared to the literature test, the laser test used a test cell length which was shorter by a factor of ten and with iodine vapor density rarer by a factor of about six. Still, the laser test could have been satisfactorily accomplished with an absorption of ten times less than the 0.54 percent loss actually measured.

Spectroscopic work in the vapor phase is of much more limited application than solution techniques because of the low volatility of most large molecules. However, should the capability of sweeping the frequency of gas lasers ever arise, the above technique may be used to increase the absorption measuring sensitivity by a factor of several orders of magnitude. Vapor phase studies would then occupy a position of in-

creasing importance.

Not much is known about the new gas lasers operating in the visible region, but development of these lasers would give impetus to usage in photochemistry. Here again, the above in-cavity technique may be useful because the much stronger intensity within the cavity may be capable of initiating measurements not otherwise possible.

SCATTERING

Turbidimetric Sedimentation

Introduction

Light can be reflected at surfaces, scattered in a medium, or absorbed as in the preceding section. When a beam of light is directed at small non-absorbing suspended particles, some of the incident radiation is scattered in all directions and the remainder is transmitted. The scattered light and the decrease of the incident beam is a function of particle size and concentration. Scattering and transmission measurements in most cases can be accomplished rapidly, and with careful application and attention to their limitation can be quite valuable in determining particle size.

Due to the availability of the low-light-loss sensitivity of the laser cavity, it was decided to determine the feasibility of using the gas laser in an in-cavity turbidimetric sedimentation configuration. Turbidimetric refers to a combination of light scattering and particle settling as a means of determining particle sizes. Expected advantages were to be smaller sample requirements through using lower concentrations and the resulting decrease in flocculation problems.

Particle sizing

Particle sizes and particle size distributions are generally measured because of the relationships they bear to other properties of the particles. Knowledge of the size characteristics of particulate material is generally of little value in itself, but particle size measurements

are often made to control the quality of the final product, because certain sizes may be correlated with certain desirable properties of the product.

Cadle (8) states that perhaps the most outstanding property of finely divided substances is the tremendous surface-to-mass ratio which they possess. Other factors being equal, the surface-to-weight ratio varies inversely with the square of the particle diameter. Thus properties of particles which depend upon the amount of exposed surface are greatly influenced by the size of the particles. The ability of particles to adsorb various substances is such a property.

Other properties which depend upon particle sizes are the solubility and rate of solution, chemical reactions, light scattering, and sedimentation. Applications wherein these properties are important occur in the paint industry, industrial hygiene, cement industry, etc.

Microscopic examination and sieving are the oldest, most direct, and simplest means for determining the size and size distribution of fine particles. Microscopic examination is tedious but gives reliable and reproducible results if careful measurements are made. The microscopic method is applicable to particles sizes from about 0.5 to 500 microns if an optical system is used, and from about 0.001 to 10 microns when electron microscopy is employed. For particle size measurements above 50 microns, sieves or screens may be conveniently employed. Sieving, which can be accomplished rather rapidly, also gives reproducible results.

Probably the most widely used method for determining the size dis-

tributions of particles in the subsieve range is based on sedimentation. Sedimentation techniques utilize the dependence of the falling velocities of particles on their size. Stokes used the principles of hydrodynamics and several simplifying assumptions to derive the equation for the force of resistance to motion of a sphere.

The scattering of light by spheres has been extensively studied, both theoretically and experimentally. In the case of non-absorbing substances, the scattering properties have been found to provide convenient measures of particle size and size distribution. The theory of scattering by a spherical particle was originally developed from Maxwell's equations by Gustave Mie in 1908. Numerous experimental measurements have amply confirmed the Mie theory. Using light scattering properties in conjunction with sedimentation is known as turbidimetric sedimentation and is one of the particular methods of interest here.

Sedimentation

When a spherical particle is left undisturbed in a medium in a gravitational field it will at first sink with increasing velocity, but when the resistance is equal to the acting force it will reach a constant velocity. At equilibrium by Stokes' law

$$6\pi r\eta v = \frac{4}{3}r^3\pi(\rho_k - \rho_f)g \qquad 31$$

where ρ_k is the density of the particles, ρ_f that of the medium, the acceleration due to gravity is g, the radius of the particle in centimeters is r, the velocity of the particle in centimeters per second

is v, and the viscosity of the medium is η. Then

$$v = \frac{2(\rho_k - \rho_f)g}{9\eta} r^2 \qquad 32$$

which for a given suspension reduces to

$$v = (\text{constant})r^2 \qquad 33$$

and for the radius of the particle

$$r = \left(\frac{9v\eta}{2(\rho_k - \rho_f)g}\right)^{\frac{1}{2}} \qquad 34$$

Sinclair (9) states that Stokes' law is correct to five percent or better for spherical particles in air with radii between one and fifty microns. For particles larger than fifty microns the velocity becomes so large that turbulence occurs, decreasing the velocity more than does the viscous drag alone. For smaller particles whose size is comparable with the mean free path of the air molecules, a correction must be applied to compensate for the tendency of the particle to slip between the air molecules, and thus move faster than predicted by Stokes' law. Test particles used in the following research have sizes well within the 1-50 micron region and therefore Stokes' law will be used without correction.

If the particle shape deviates considerably from sphericity, then Stokes' law cannot be expected to give the exact relation between the time of settling and the particle size. It has been shown that the law holds reasonably well, within the limits of experimental error, also for certain types of nonspherical particles. Irani (10) states that Stokes' law can usually be utilized for particles whose maximum-to-minimum

diameter ratio does not exceed four. Particles which are not spherical may be regarded as having an effective Stokes' radius equal to that of a sphere of the same density and having the same terminal velocity.

Stokes' law is concerned only with terminal velocity. A certain time must elapse after a particle starts to settle before the terminal velocity is reached. Fortunately, this time is negligible compared with the settling times involved in particle size determinations for particles in the subsieve range.

The particles should fall as they would in a medium of unlimited extent. The walls of the container should have a negligible effect on the sedimentation velocity. For particles in the subsieve range, the walls of vessels over one centimeter in diameter have a negligible effect. Particle concentration is also important. The maximum volume concentration of particulate material which can be used without appreciably affecting the results seems to be about one percent. Otherwise, interference between the particles becomes important. In addition, the viscosity of the medium ceases to be that of the pure fluid.

Turbidity

Turbidity is another name for photo-extinction and since photo-extinction seems to be more descriptive, it is the nomenclature that will be used. The photo-extinction method of particle size determination is very simple in principle. If a beam of light is passed through a suspension, the attenuation of the light produced by the suspended particles is a function of the concentration and the size of the particles. Thus a beam of light can be used as the analytical tool for determining

concentration or size depending on which one is initially known. There are numerous advantages to using such a method. Very dilute suspensions can be used and thus very small amounts of powder can be studied. The suspension is not disturbed by this type of sampling method. The necessary data is obtained rapidly and can easily be continuously recorded. The beam of light can be made very narrow relative to the height of the suspension in the sedimentation chamber, thus decreasing errors resulting from uncertainties in the sedimentation distance. Photo-extinction is almost always used in conjunction with sedimentation and is usually called turbidimetric sedimentation.

Unfortunately, the photo-extinction method has two major disadvantages. The first is that conversion of the original data to a size frequency distribution is at best a tedious job. The attack on this drawback in this dissertation is to use digital computer techniques along with a simpler sedimentation setup made possible by the high sensitivity of the laser light-loss detection system. The second disadvantage is that the basic theory which must be applied when dealing with materials having a wide particle size distribution is very complicated due to the variation of scattering with respect to particle size. On this matter, a new method of determining size frequency distributions is developed in which the detected output change is recorded in such a manner that there isn't any dependence between size and scattering. Much more will be said on this later.

The theory behind the photo-extinction method is based on the same kind of reasoning as was developed in the absorption section. It is

developed by the application of the Lambert-Beer law to a suspension of solid particles in a fluid medium. Cadle (8) gives as an applicable form of the Lambert-Beer law

$$I = I_o e^{-AKl} \qquad 35$$

where A is the projected area per unit volume, l is the path length over which scattering takes place, K is the total scattering coefficient and is equal to the effective scattering cross-section divided by the geometric cross-section. The product AK is called the turbidity or extinction coefficient.

The total scattering coefficient K is troublesome since it has been found to be dependent on particle size. Rose (11) states that K varies between one and four for particles with diameters between one and five microns. However, he also indicates that K is approximately equal to two for the size range of 5 to 25 microns which is the region of interest for the following work. The theoretical limiting value of K as the particle size increases is two. However, as the size increases, the proportion of the scattered light which is scattered in a forward direction becomes sufficiently great that a part of the scattered light is measured along with the transmitted light making the limiting value of K unity. Rose (11) gives as a requirement for using his scattering coefficient curve that the solid angle subtended by the transmission detector be near or less than 0.00024 solid radians.

Experimental Setup

Figure 13 is a photograph of the experimental arrangement used in this experiment. It consists of the aforementioned gas laser cavity with the calibrating VBAF between the right-hand mirror and discharge tube while the sedimentation cell is between the left-hand mirror and discharge tube. Because of the previous explanation about the VBAF, little need be said here except that using it provides the method of determining the total scattering losses.

The sedimentation chamber is somewhat unique in that the particles do not initially fill the whole chamber. They are first of all forced into an upper insertion chamber consisting of a long entrance neck for dispersion, small holes in the top for air stabilization, and a sliding door in the bottom for entrance into the sedimentation chamber. This particular geometry evolved from the need to avoid covering the Brewster-angle windows in the sedimentation chamber with test particles during the initial insertion. The Brewster-angle windows are necessary so as to provide a stable sedimenting environment and yet pass the cavity beam with minimum losses. This particular type of arrangement gives rise to what may be called layered settling.

The apparatus to the left of the laser in Figure 13 is a commercially available S. S. White airbrasive unit intended for specialized cutting operations. Cutting action is performed by the impingement of sharp-edged abrasive particles. These particles are propelled through a small nozzle from a vibrating powder chamber with small holes in a bottom orifice plate. Therefore, an instrument of this type provides both the vibrating sieve and small nozzle requirements of a good dis-

Figure 13. Laser photo-extinction system

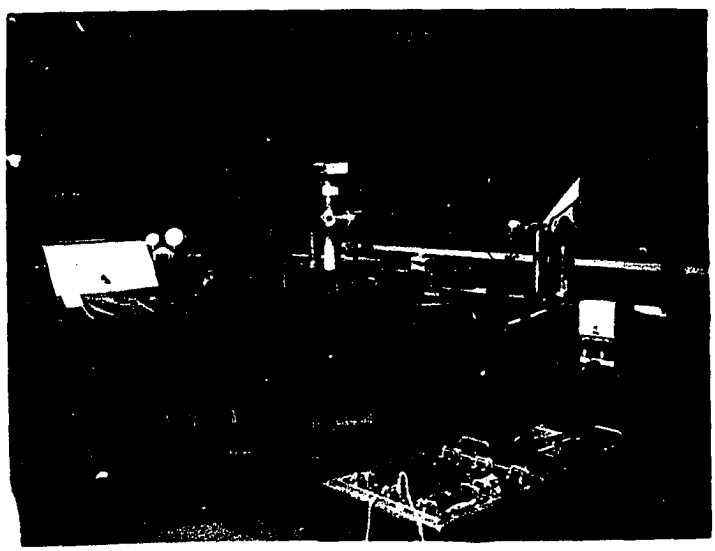

persing agent for powder into air.

Layered settling

Irani (10) states that Marshall (12) was the first to use the layered settling technique wherein the particulate matter is concentrated in a layer whose thickness is small compared to the distance below the surface at which the amount settled is measured. With such an arrangement Stokes' law can be used directly to determine particle size distributions. This is because, by Stokes' law, the rate of fall of particles is proportional to the diameter squared so that larger particles fall more rapidly. Due to this, the size of particles present in the sedimentation chamber at a particular level is essentially uniform provided that the level is sufficiently removed from the initial concentration. Irani (10) also states that although the layer method is intuitively simple and straight-forward, no completely adequate apparatus has been yet developed.

No known work has been published utilizing photo-extinction in conjunction with the layered sedimentation principle. The probable reason for this is that by the time the particles reach the beam, the particle concentration is only a fraction of what it initially was when inserted. Therefore, it would be extremely difficult to disperse an initial concentration dense enough to still provide an appreciable light loss at the beam measuring level. Use of the 6328 angstrom gas laser as a low-light-loss detector overcomes this problem thereby making this method feasible in principle at least.

Particle size distributions

Most particulate matter can be classified as following one of the two most applicable size frequency distributions. The first of these to be considered is the familiar normal distribution function as represented by

$$f(d) = \frac{1}{s\sqrt{2\pi}} \exp\left\{-\frac{1}{2}\left(\frac{d-\bar{d}}{s}\right)^2\right\} \qquad 36$$

where $\bar{d}$ is the arithmetic mean and s the standard deviation. The arithmetic mean is given by equation 37 and the standard deviation by equation 38.

$$\bar{d} = \frac{\sum n_i d_i}{N} \qquad 37$$

$$s = \left\{\frac{\sum (d_i - \bar{d})^2 n_i}{N}\right\}^{\frac{1}{2}} \qquad 38$$

Particulate matter with a size distribution corresponding to the normal distribution is usually only produced by chemical processes involving condensation or precipitation.

The second, more frequently encountered, size distribution is called the log-normal distribution and is given by

$$f(d) = \frac{1}{\ln s_g \sqrt{2\pi}} \exp\left\{-\frac{1}{2}\left(\frac{\ln d - \ln d_g}{\ln s_g}\right)^2\right\} \qquad 39$$

where d_g is the geometric mean and s_g the geometric standard deviation. The geometric mean is defined by equation 40 and the geometric standard deviation by equation 41.

$$\ln d_g = \frac{1}{N} \sum n_i (\ln d_i) \qquad 40$$

$$\ln s_g = \left\{ \frac{\sum n_i (\ln d_i - \ln d_g)^2}{N} \right\}^{\frac{1}{2}} \qquad 41$$

Particulate matter formed by a milling, grinding, or crushing process appears to be governed very often by the log-normal law.

There are other size frequency distributions that fit particular situations but these will not be used due to the large area covered by the above two forms.

Theoretical results

Figure 14 illustrates the geometry of the sedimentation and insertion chambers. At any instant of time t the size of the particles in the beam will depend on the distance that they have fallen from their initial position in the insertion chamber. If the initial concentration, N, and the size frequency distribution, f(d), are known, it is possible to calculate the projected area per cubic centimeter at the beam at time t. To do this it is necessary to relate the distance from the insertion chamber levels to the laser beam to the corresponding diameter at these levels that will sediment to the beam at time t. Equation 42 relates speed to diameter while equation 43 relates distance to speed and time.

$$v = 3(10^5)\rho d^2 \qquad 42$$

Here ρ = specific density, d = diameter in centimeters, and v = velocity in centimeters per second.

$$x - x_i = vt \qquad 43$$

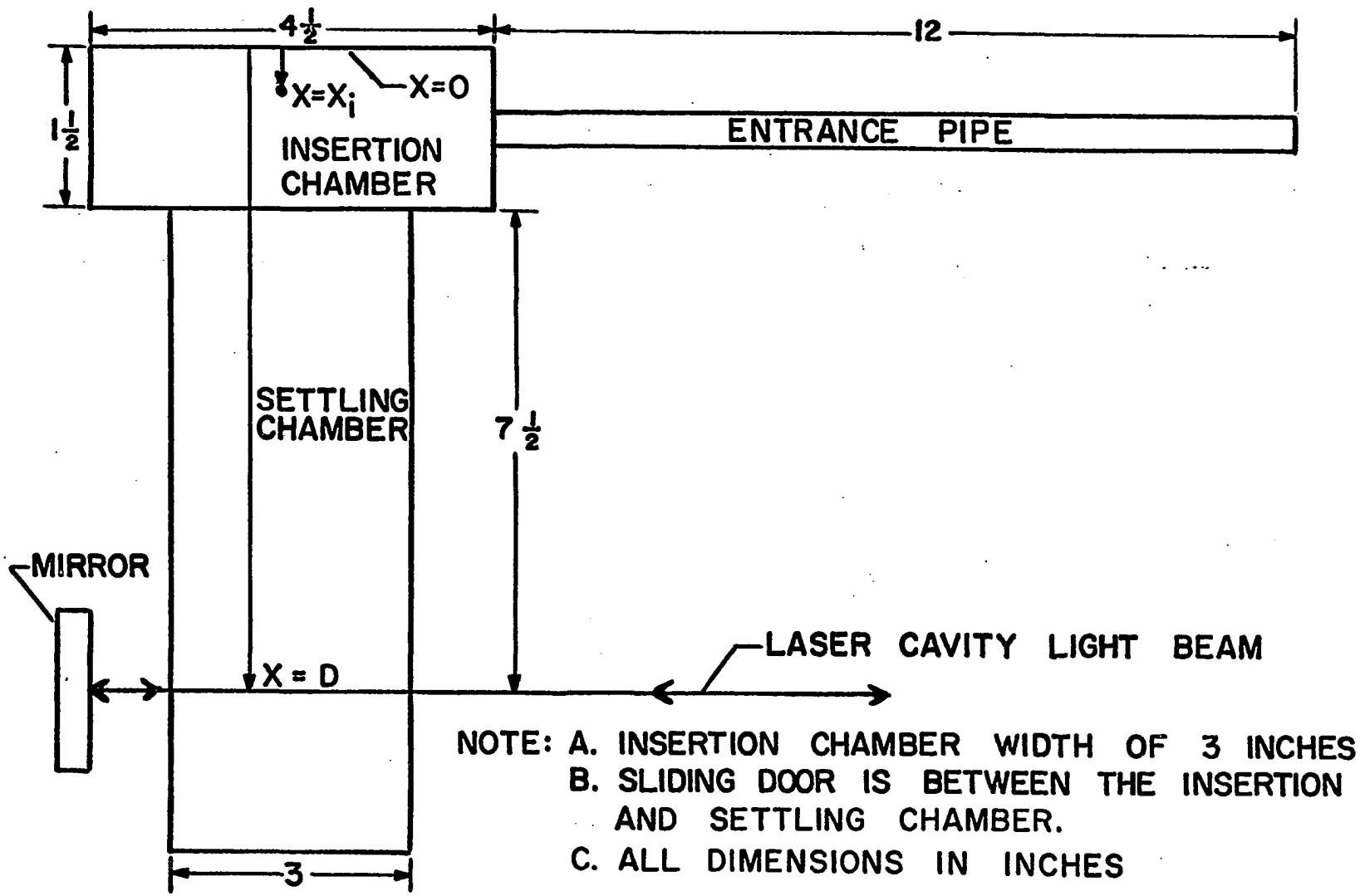

Figure 14. Sedimentation and insertion chambers

The distance from the insertion chamber points x_i to the beam at $x = D$ is given by $D - x_i$. Solving for d in equation 42 and v in equation 43 and combining, results in

$$d = \left(\frac{D - x_i}{3(10^5)\rho t}\right)^{\frac{1}{2}} \qquad 44$$

Multiplying f(d) by N, the insertion chamber concentration per unit volume, results in an expression giving the relative number of particles having a particular size. Integrating Nf(d) between any two sizes gives the total number of particles per unit volume with diameters between the two sizes. Multiplying by $\pi d^2/4$ gives the projected area per unit volume of the particles with diameters between the two sizes. Therefore, multiplying f(d) by N and $\pi d^2/4$, substituting equation 44 for d, and integrating on x_i from zero to $x_i = 3.81$ centimeters results in the projected area per unit volume in the beam at any time t. This is the parameter A that is needed to solve the Lambert-Beer equation 35.

Equation 45 represents the projected area per unit volume at the beam at time t for a normal distribution while equation 46 does the same for a log-normal distribution.

$$A = \int_{x_i = 0}^{x_i = 3.81} \frac{\pi}{240\rho t}\left(\frac{D - x_i}{3(10^5)\rho t}\right)^{\frac{1}{2}} \frac{N}{\sqrt{2\pi}\, s} \exp\left\{-\frac{1}{2}\left(\frac{10^4\left(\frac{D - x_i}{3(10^5)\rho t}\right)^{\frac{1}{2}} - \bar{d}}{s}\right)^2\right\} dx_i \qquad 45$$

$$A = \int_{x_i = 0}^{x_i = 3.81} \frac{\pi}{24(10^5)\rho t\sqrt{2\pi}\ln s_g} \frac{N}{} \exp\left\{-\frac{1}{2}\left(\frac{\ln 10^4\left(\frac{D - x_i}{3(10^5)\rho t}\right)^{\frac{1}{2}} - \ln d_g}{\ln s_g}\right)^2\right\} dx_i \qquad 46$$

To get the resulting percent loss at time t, it is necessary to use the Lambert-Beer equation

$$I = I_o e^{-AKl} \tag{47}$$

$$\% \text{ loss} = (1 - e^{-AKl})(100) \tag{48}$$

Therefore, it is possible to get percent loss versus time by integrating equation 45 or 46 and substituting the resulting A into equation 48. To integrate equation 45 or 46 it is necessary to use digital computer techniques. Figures 15 through 20 illustrate percent loss versus time results with variations caused by changing some of the parameters such as concentration, density, sedimentation distance, and distribution parameters. Observation of these theoretical results helps to interpret any experimentally obtained data.

Experimental results

To test the feasibility of using the gas laser cavity in photoextinction, test particles were loaded into the mixing chamber of the airbrasive unit. Before forcing particles into the insertion chamber, the gas laser was calibrated for losses by varying the VBAF angle and noting the laser output as indicated on the Sanborn recorder in Figure 13. The percent loss for all VBAF angles and therefore laser outputs is known. Therefore, after the sedimentation run, the recorder curve can be converted to percent loss and an experimental percent loss curve for an unknown particle sample can be obtained.

First, the recorder drive was energized so as to take up the slack in the paper and have it moving continuously. Next, in rapid succession,

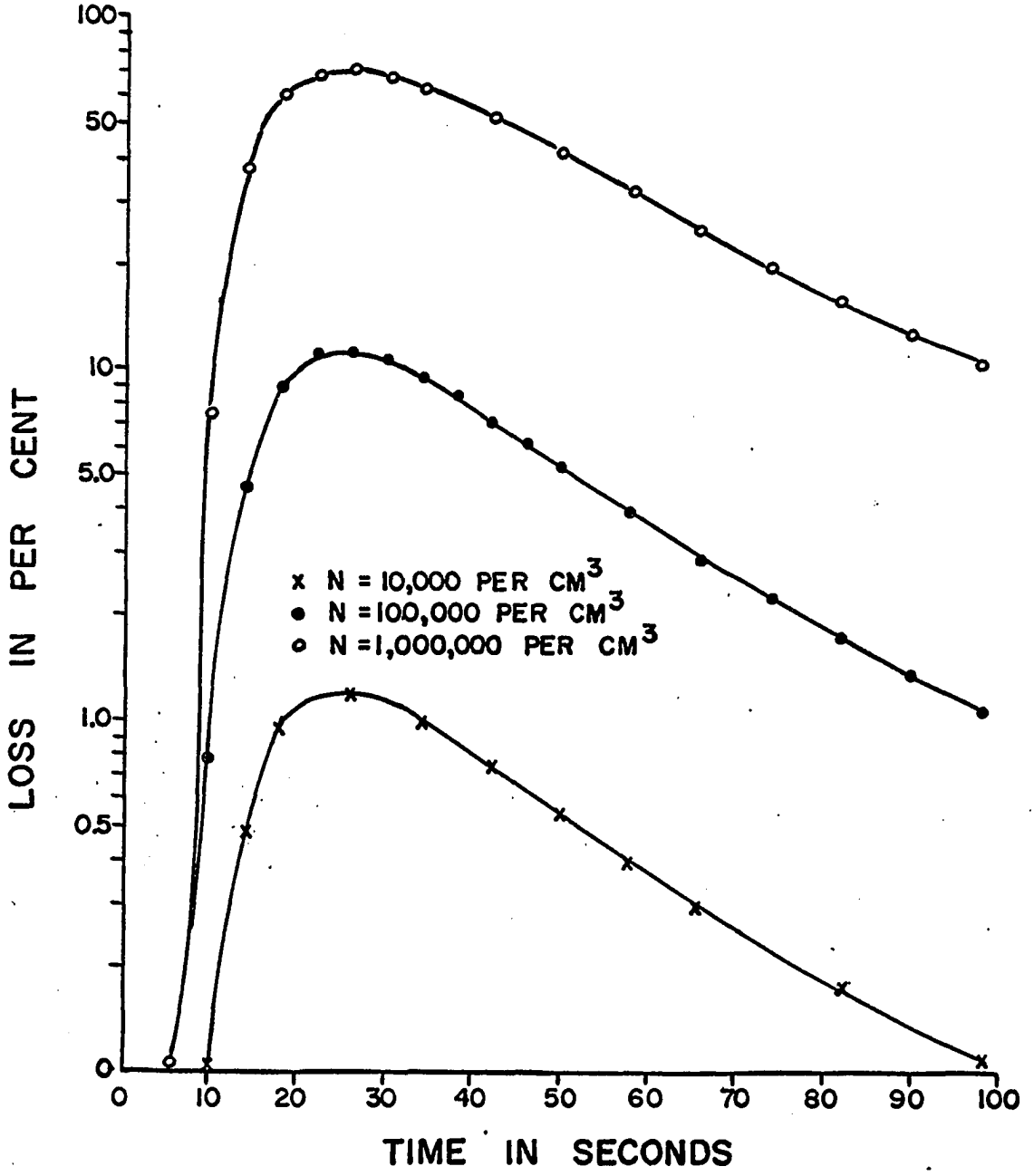

Figure 15. Normal distribution concentration effects. D = 22.86 cm. $\rho = 2.5$. $\bar{d} = 8.5$ microns. s = 2.75.

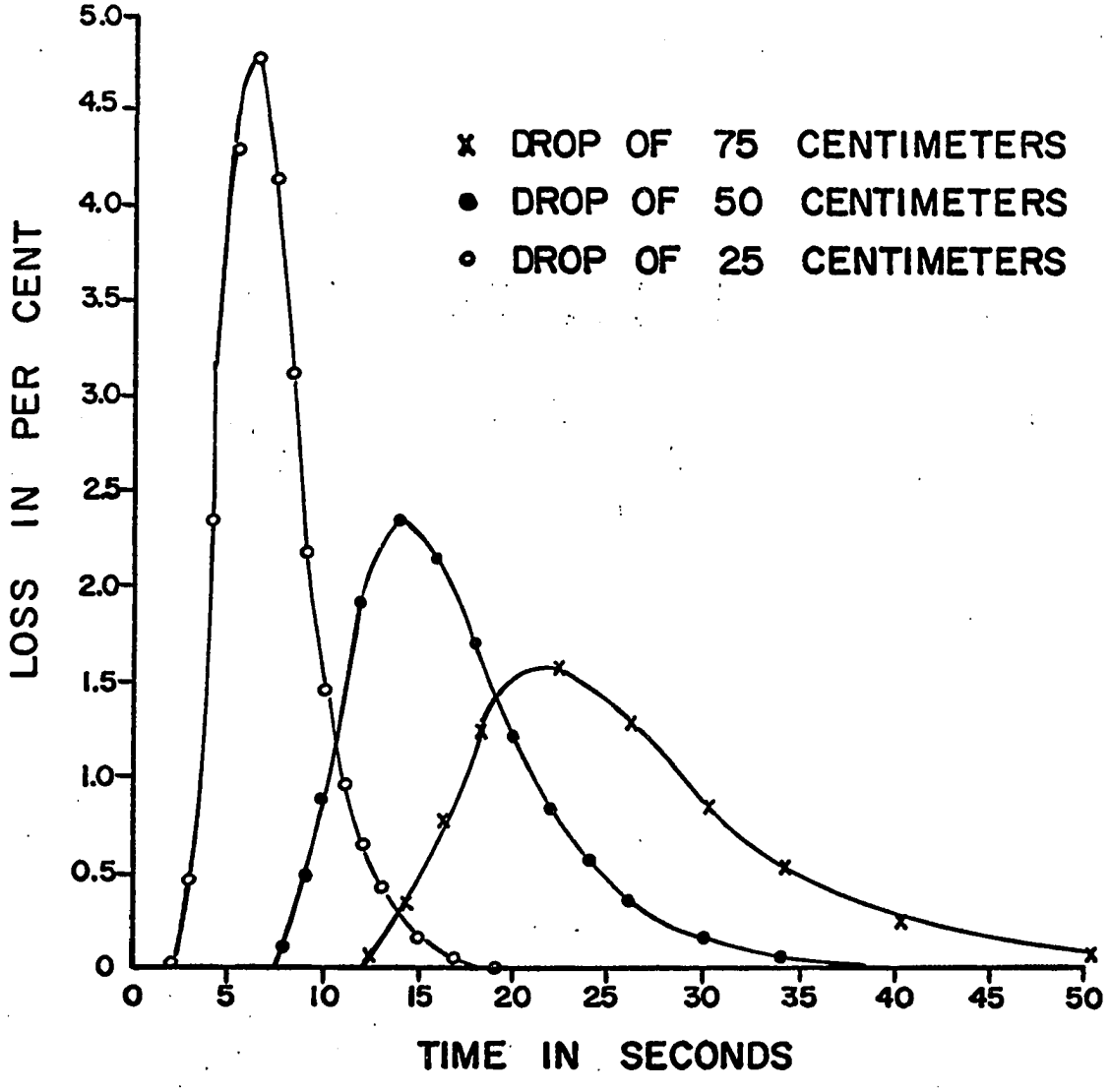

Figure 16. Normal distribution sedimentation distance effects. $N = 5000$ per cm^3. $\bar{d} = 20$ microns. $s = 3.0$. $\rho = 2.5$.

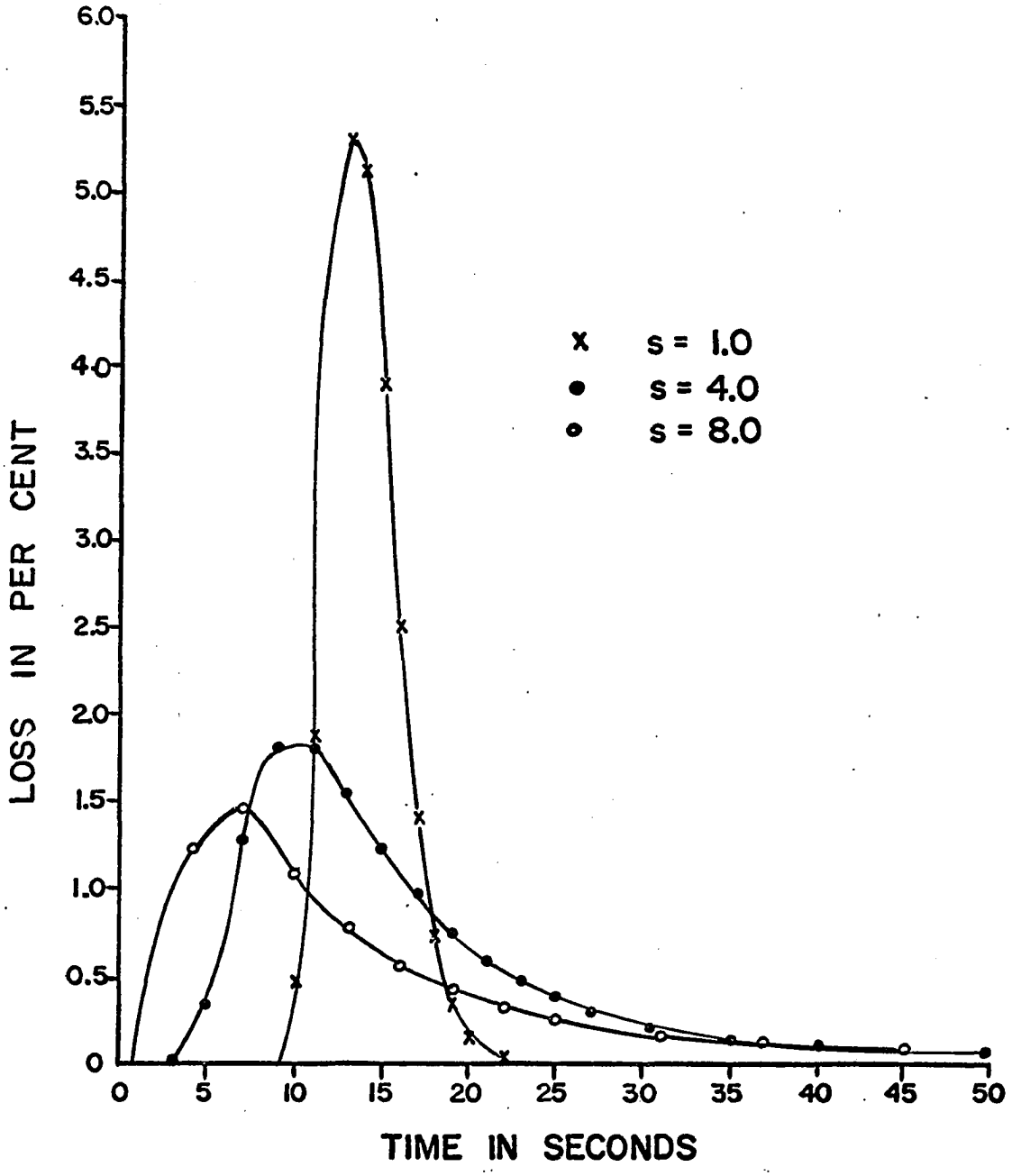

Figure 17. Effects of varying the standard deviation parameter s of a normal distribution. N = 5000 per cm^3. ρ = 2.5. $\bar{d}$ = 15 microns. D = 25 cm.

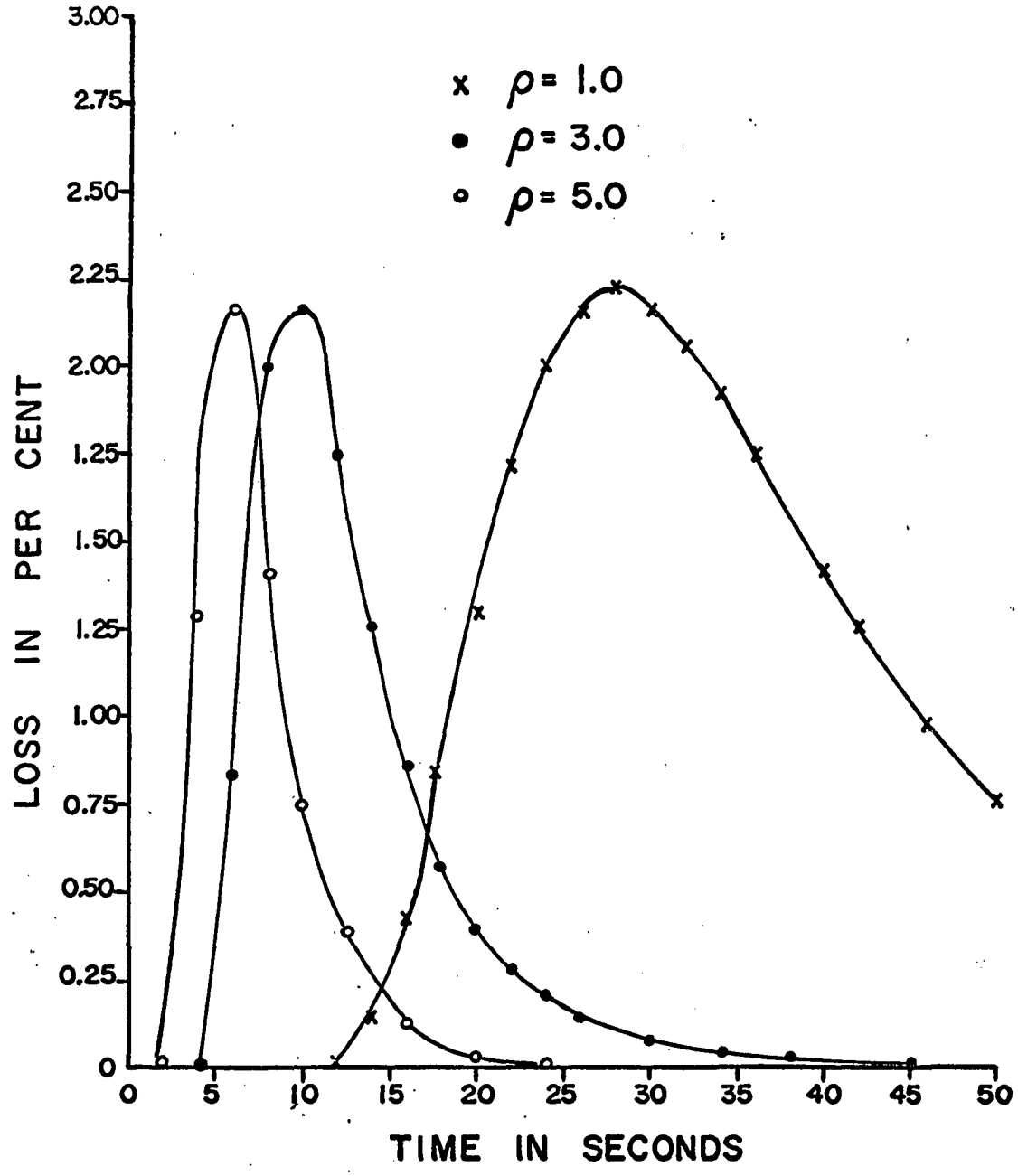

Figure 18. Normal distribution particle density effects. N = 5000 per cm^3. $\bar{d}$ = 15 microns. s = 3.0. D = 25 cm.

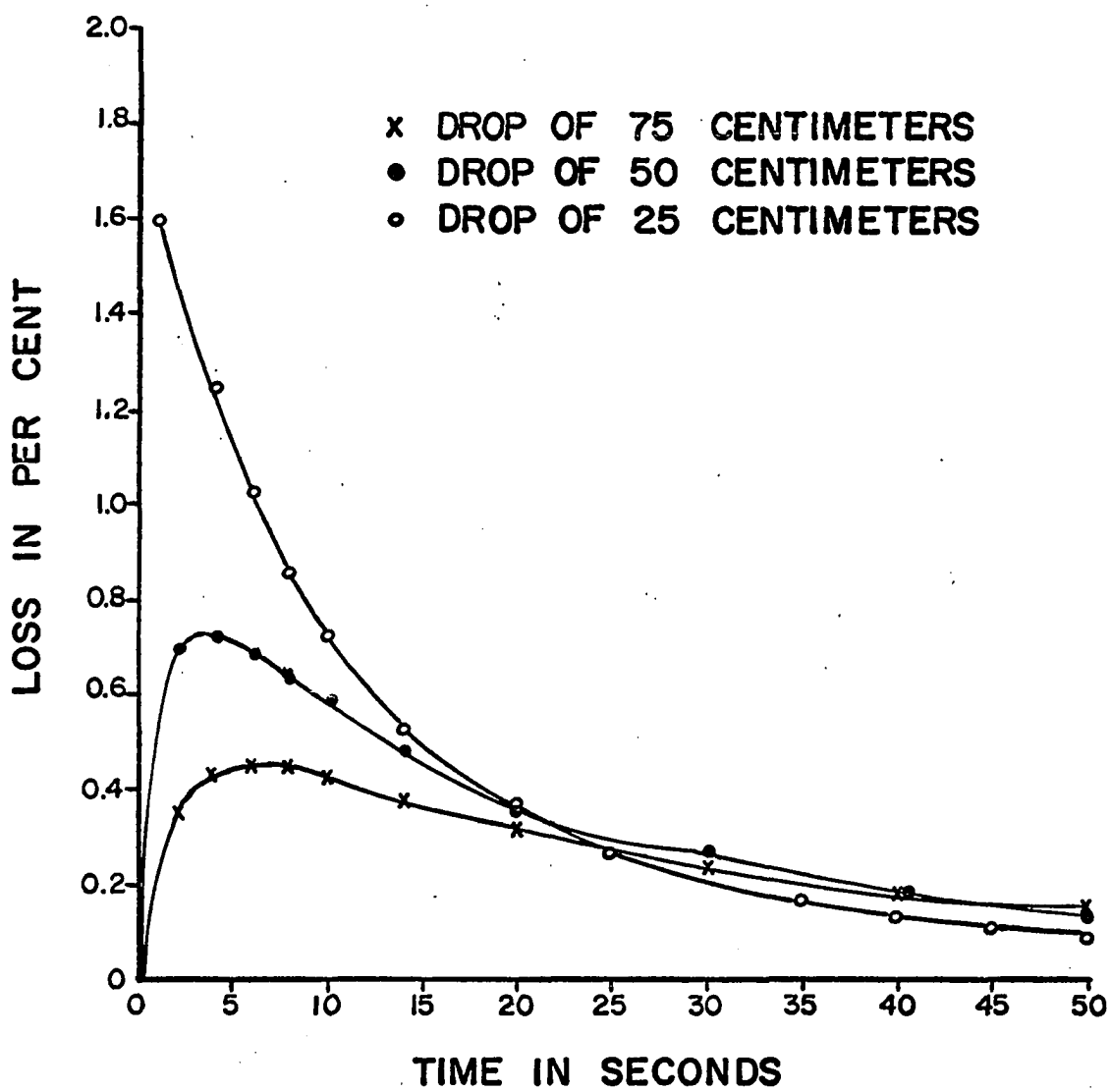

Figure 19. Log-normal distribution sedimentation distance effects. N = 5000 per cm^3. $\ln d_g = 2.7$. $\rho = 2.5$. $\ln s_g = 0.7$.

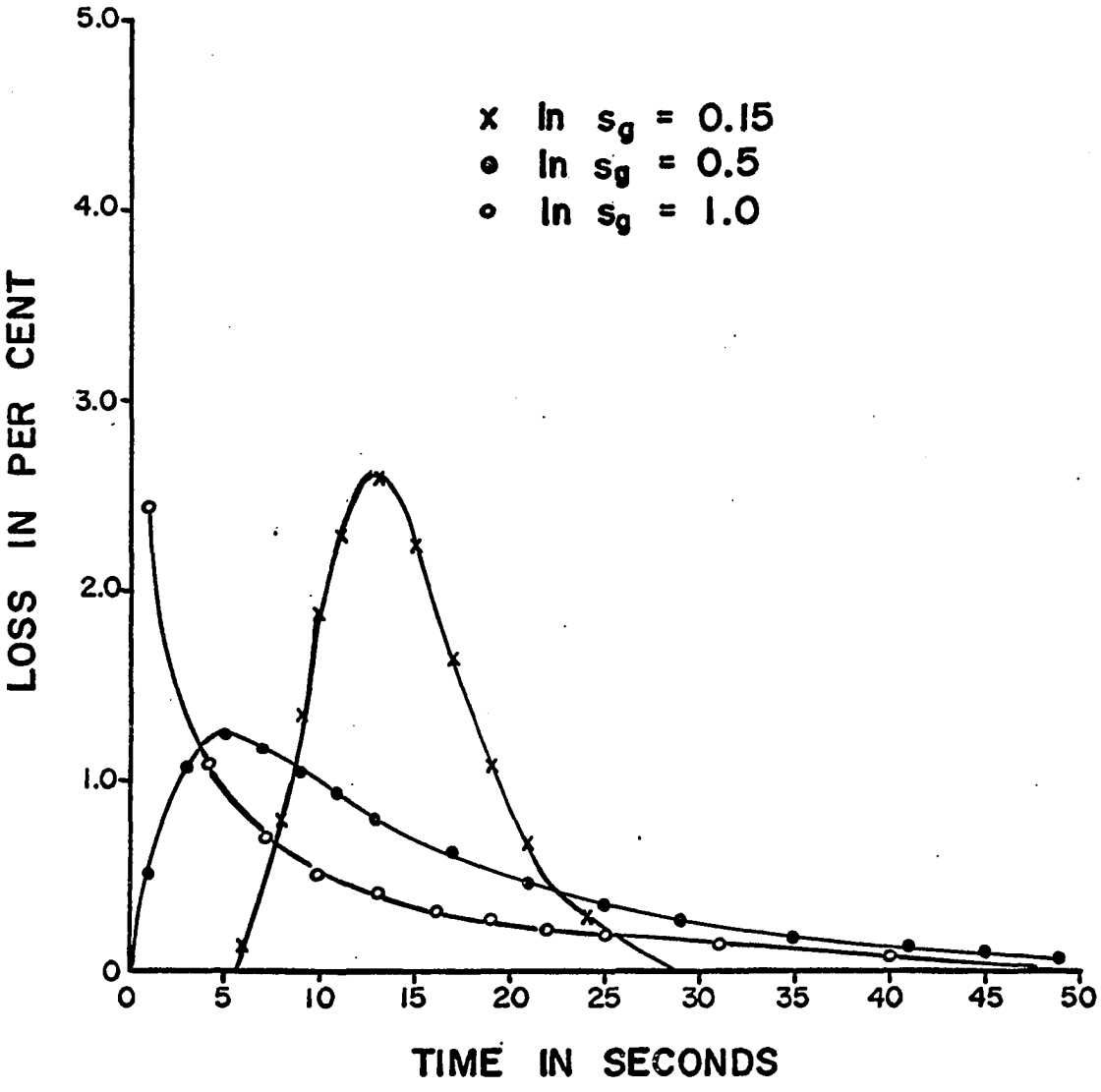

Figure 20. Effects of varying the geometric standard deviation parameter of a log-normal distribution. N = 5000 per cm^3. ln d_g = 2.7. ρ = 2.5. D = 25 cm.

the particles were forced into the insertion chamber, the slide door pulled, and the timing marker switch flipped on the Sanborn recorder. These actions took about 2-3 seconds and this amount of time has to be added to the timing marks on the recorder output to correct the time scale. The largest particles reach the beam first and cause a fairly rapid laser output change due to the speed with which the concentration increases. The latter parts of the run have slower associated output variations because smaller particles are involved and their sedimentation rates are much slower.

As stated above, once the recorder curve is obtained, it can be converted to percent loss versus time. To get the size frequency distribution of the test particles, it is only necessary to use the percent loss figure in equation 49.

$$w = \% \text{ loss} = (1 - e^{-AKl})(100) \qquad 49$$

Equation 49 can be solved for A, the projected area per cubic centimeter; since K, the total scattering coefficient; and l, the path length, are known.

$$A = \frac{-\ln\left(1 - \frac{w}{100}\right)}{Kl} \qquad 50$$

The projected particle area in square microns per cubic centimeter is $10^8 A$. The number, n, of particles per cubic centimeter present at time t in the beam is

$$n = 10^8 A/\text{average particle area} \qquad 51$$

Note that here an average particle cross-sectional area has to be used since there isn't any way of knowing, yet, just what distribution gave

rise to this particular percent loss figure. To determine possible errors arising from this step, a short computer program was run calculating the arrival and departure times of the insertion chamber cross-section corresponding to a particular particle diameter. The results are tabulated in Table 2 and as can be seen, the results show that only a very small particle diameter spread is present at any one time.

Table 2. Arrival and departure times of insertion chamber cross-sections at the beam for particles with a specific density of 2.5

Particle diameter in microns	Arrival time in seconds	Departure time in seconds
1	2540.00	3048.00
2	635.00	762.00
3	282.22	338.67
4	158.75	190.50
5	101.60	121.92
6	70.56	84.67
7	51.84	62.20
8	39.69	47.62
9	31.36	37.63
10	25.40	30.48
11	20.99	25.19
12	17.64	21.17
13	15.03	18.04
14	12.96	15.55
15	11.29	13.55
16	9.92	11.91
17	8.79	10.55
18	7.84	9.41
19	7.04	8.44
20	6.35	7.62
21	5.76	6.91
22	5.25	6.30
23	4.80	5.76
24	4.41	5.29
25	4.06	4.88
26	3.76	4.51
27	3.48	4.18
28	3.24	3.89

Therefore,

$$n = \frac{4(10^8)A}{\pi d^2} \qquad 52$$

where

$$d^2 = 10^8\left(\frac{20.995}{3(10^5)\rho t}\right) \text{ microns}^2 \qquad 53$$

Choosing the distance as 20.955 centimeters from the insertion chamber center further reduces any error caused by assuming an average diameter. Finally,

$$n = \frac{-4(10^8)\ln\left(1 - \frac{w}{100}\right)}{Kh\pi d^2} \qquad 54$$

Summarizing, to get the size frequency distribution it is necessary to read the percent loss curve versus time, calculate the corresponding diameters, solve equation 54, and plot n versus diameter.

To calculate the initial insertion chamber concentration, N, the value of n must be multiplied by the corresponding sedimentation speed at that time and the resulting curve integrated and divided by 3.81 centimeters to allow for the insertion chamber depth.

$$v = \frac{20.995}{t} \text{ cm/sec} \qquad 55$$

$$vn = \frac{-4(20.995)(10^8)\ln\left(1 - \frac{w}{100}\right)}{Kl\pi d^2 t} \qquad 56$$

$$N = \frac{1}{3.81}\int^{\infty} vn\, dt \quad \text{particles/cm}^3 \qquad 57$$

A computer program was devised to handle the data accumulated from running some of the above tests. Due to the wide variation in the types of percent loss curves that can be encountered, it was necessary to put

some flexibility into the program. This was best accomplished by inserting the initial time desired for the first percent loss reading, the last time a reading is desired, and the time decrement between readings as data tape items. This allows choosing any time interval, broken up into as many readings as necessary.

If the resulting size frequency distribution curve is known to be log-normal or normal, as would be expected in many cases, there would be some advantage to automatically calculating the distribution parameters. This can be done in the computer program by first adding up all values of n. Then, as Dallavalle (13) states, if the distribution is normal, the arithmetic mean $\bar{d}$ and standard deviation s can be determined by

$$\bar{d} = 50 \text{ percent size} \tag{58}$$

$$s = 84.13 \text{ percent size} - 50 \text{ percent size} \tag{59}$$

$$= 50 \text{ percent size} - 15.87 \text{ percent size} \tag{60}$$

If the distribution is log-normal, the geometric mean d_g and geometric standard deviation s_g can be determined by

$$d_g = 50 \text{ percent size} \tag{61}$$

$$s_g = \frac{84.13 \text{ percent size}}{50 \text{ percent size}} = \frac{50 \text{ percent size}}{15.87 \text{ percent size}} \tag{62}$$

Equations 58 through 62 can be easily solved in the computer program by simply adding successive values of n until the resulting percentage figures of the total are arrived at. Then the resulting diameters are computed and outputted.

Before outputting any of the computer data it is desirable to first normalize the resulting values of n to some value, say 1000. Then, data

for more than one run can be compared without the resulting scale differences. This can be accomplished in the computer program by the procedure of taking the first value of n and comparing it with all other values; multiplying it by the factor necessary to make it 1000, if it was the largest, and multiplying all other values of n by the same factor; or taking the next number n and repeating the above procedure if it was smaller than some other value of n.

Figures 21 through 24 represent size frequency curves for four particulate materials that were tested. In each case a comparison is made against a microscopic size analysis of the material. Figures 25 through 28 consist of the laser output curves recorded as a function of time on a Sanborn recorder from which the data was taken to construct Figures 21 through 24.

The test material for Figure 21 consists of 0-10 micron diameter glass spheres. Note that there is a decided offset error of about three microns towards larger diameters. The same offset is again evident in Figure 22 on 10-20 micron diameter glass spheres. The size frequency curves for both of these test materials were highly reproducible and always, the same offset was encountered. The most probable cause is the tendency of larger particles to attenuate cavity oscillations more than their geometrical scattering cross-sections would indicate. This would cause the system to respond with an output falsely indicating that more large particles were present than actually were. The first indication that something like this might be happening was when a slightly pulsating output was observed during the initial tests. This was thought

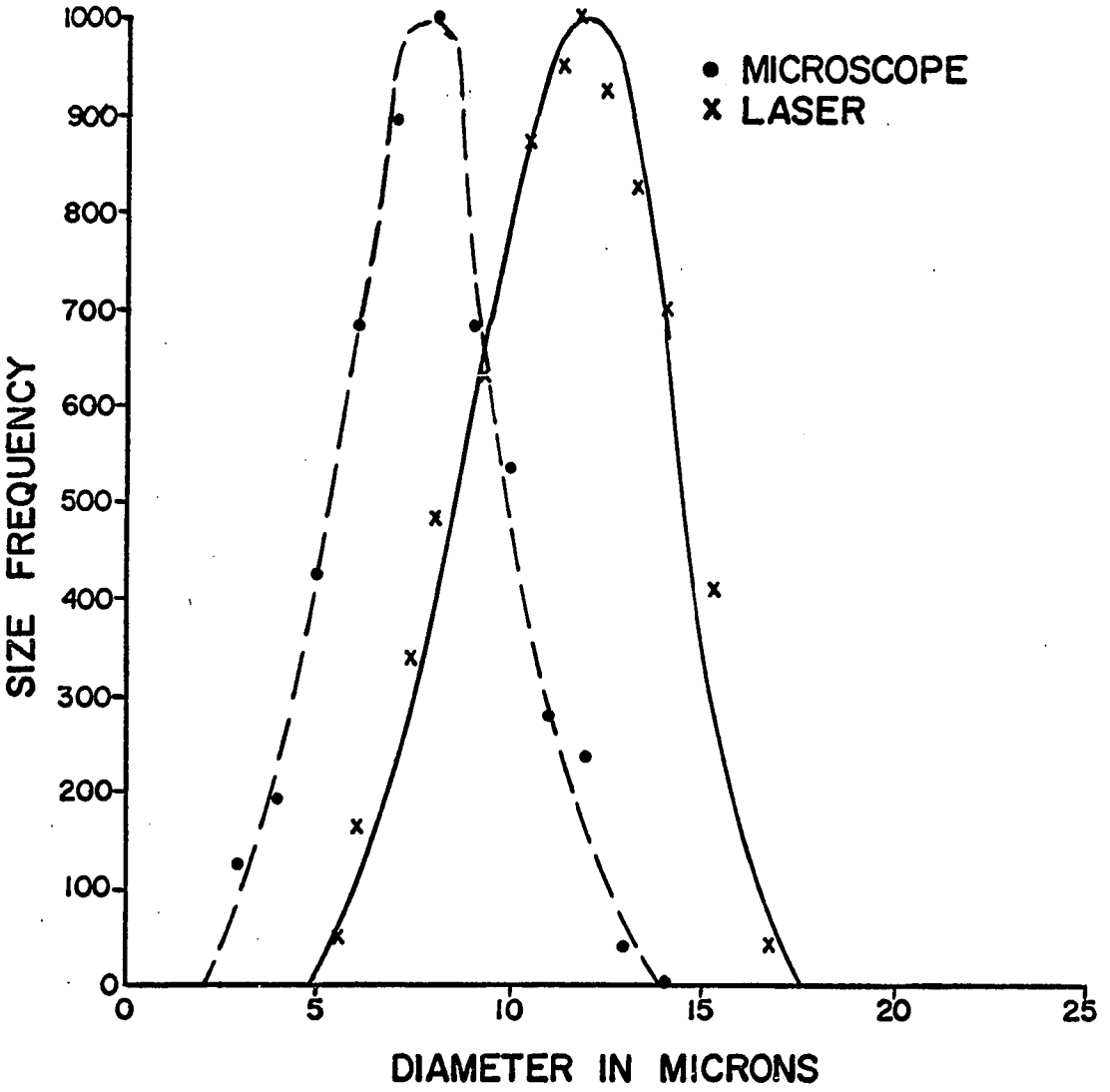

Figure 21. Photo-extinction test results for 0–10 micron glass spheres

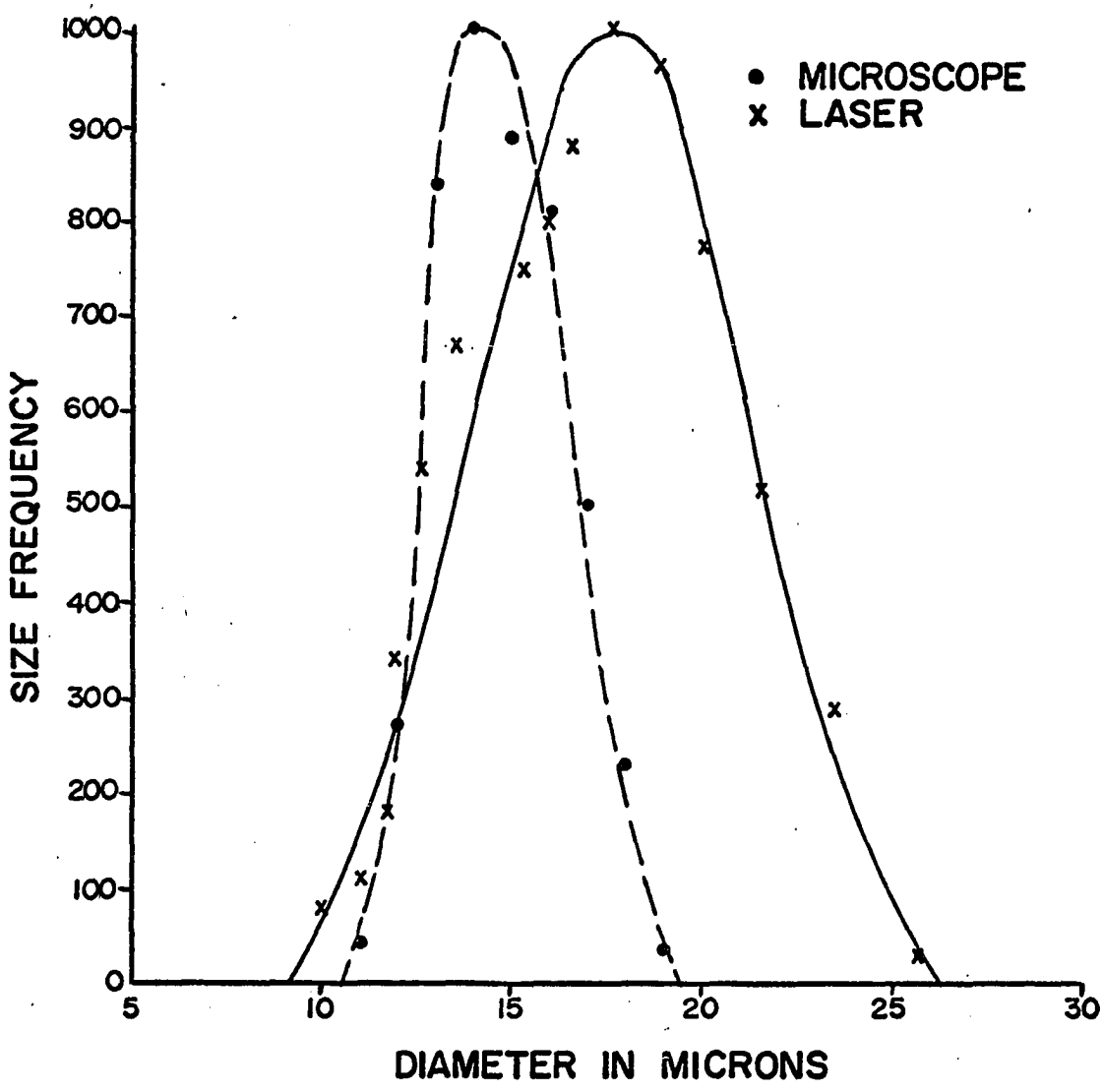

Figure 22. Photo-extinction test results for 10-20 micron glass spheres

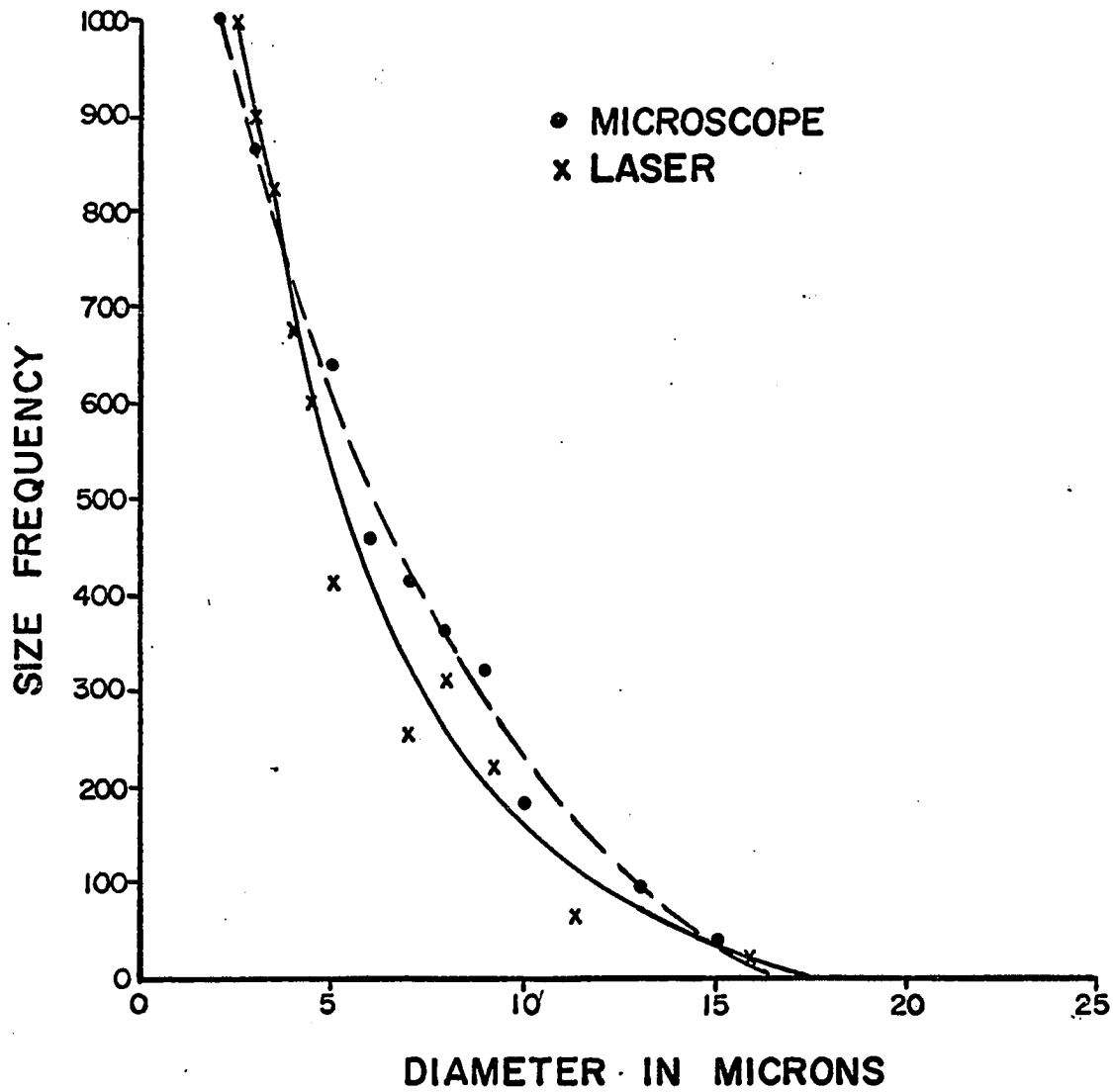

Figure 23. Photo-extinction test results for talc particles

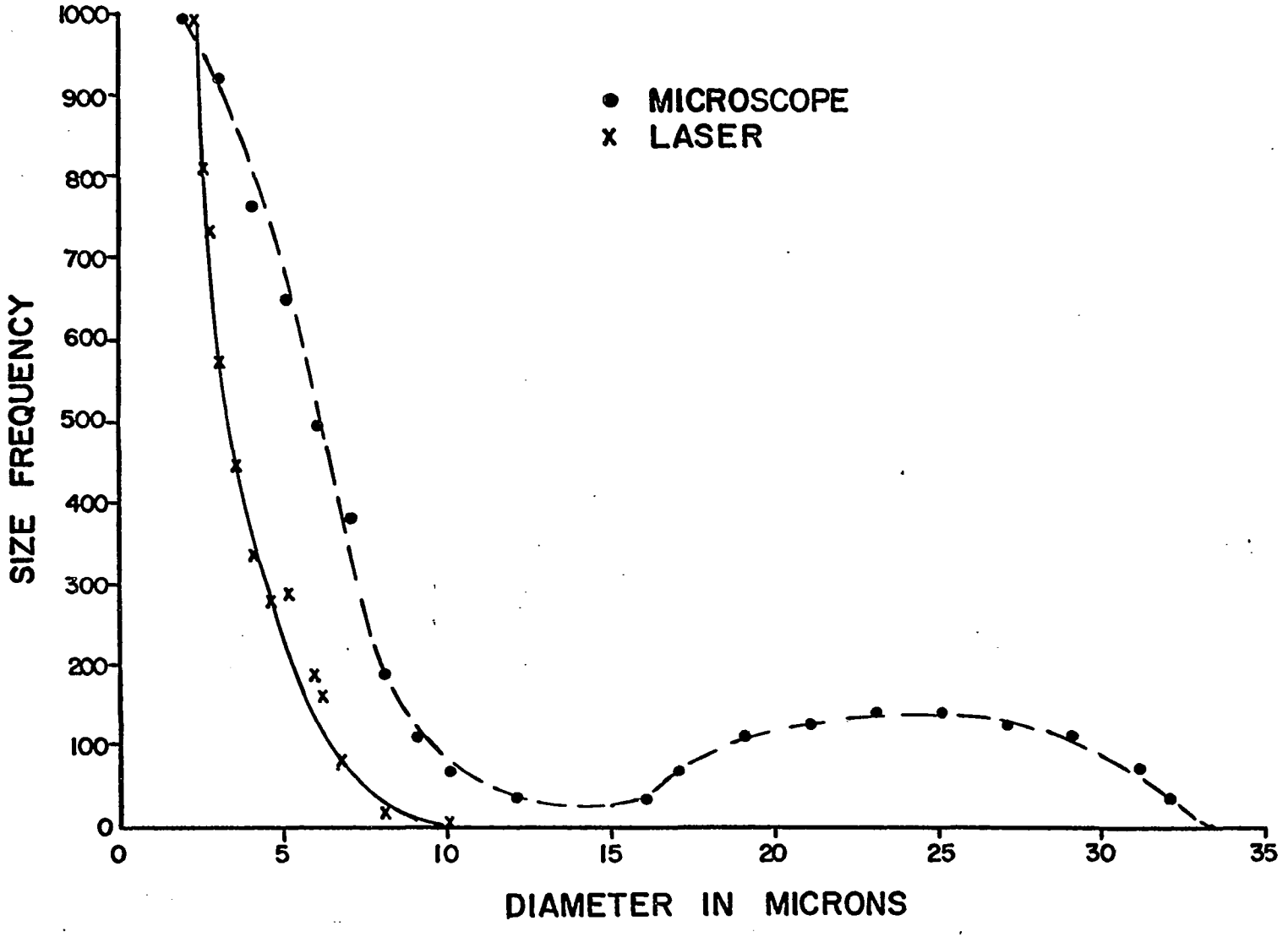

Figure 24. Photo-extinction test results S. S. White airbrasive powder

Figure 25. Sanborn recording of photo-extinction test on 0-10 micron glass spheres

Figure 26. Sanborn recording of photo-extinction test on 10-20 micron glass spheres

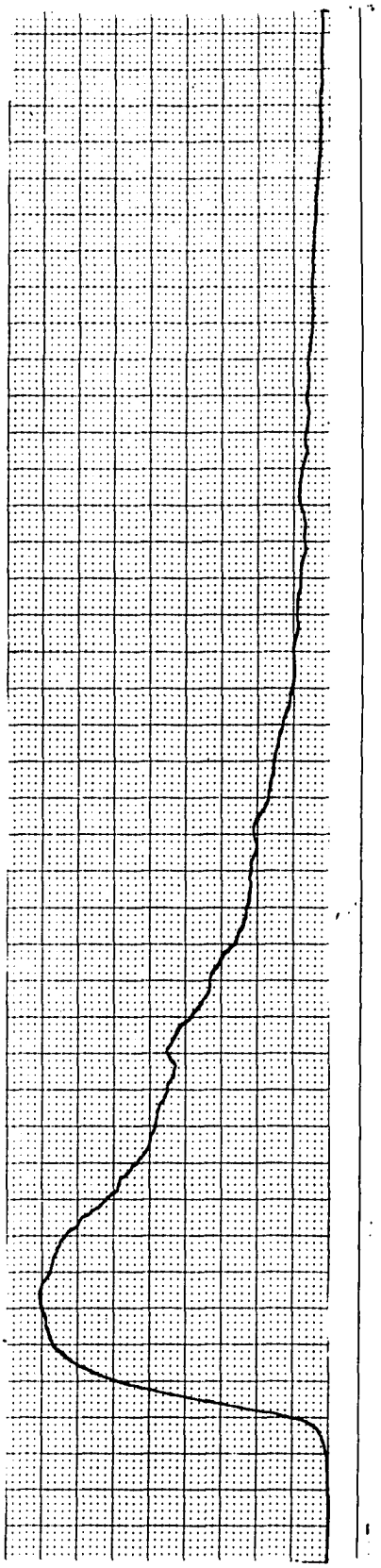

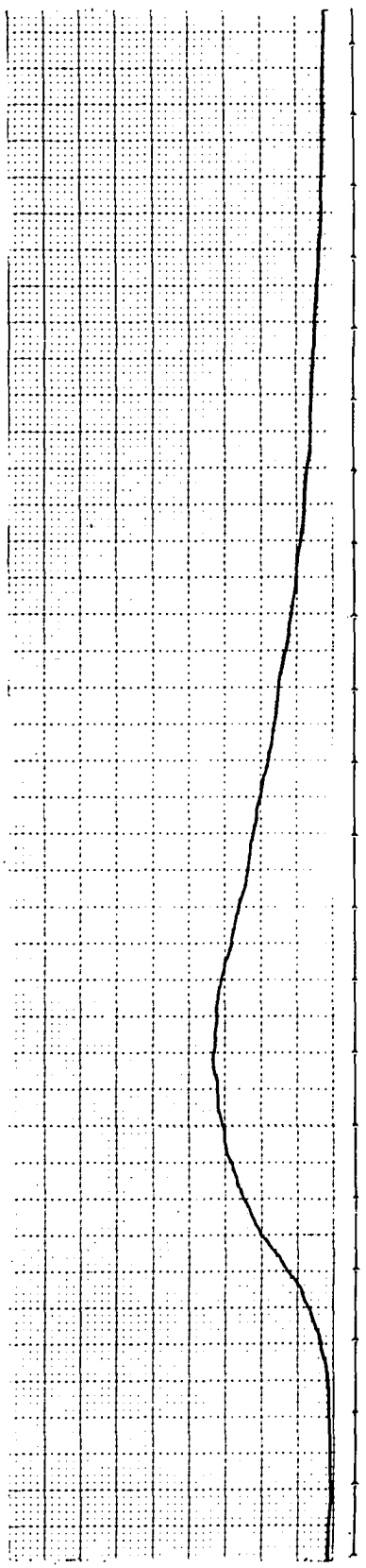

Figure 27. Sanborn recording of photo-extinction test on S. S. White airbrasive particles

Figure 28. Sanborn recording of photo-extinction test on talc particles

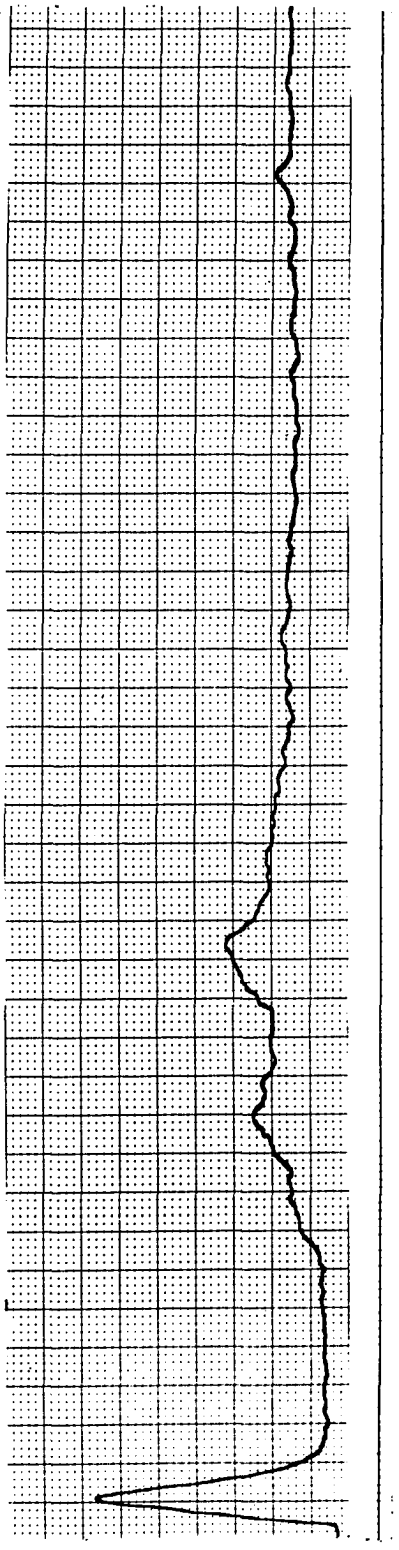

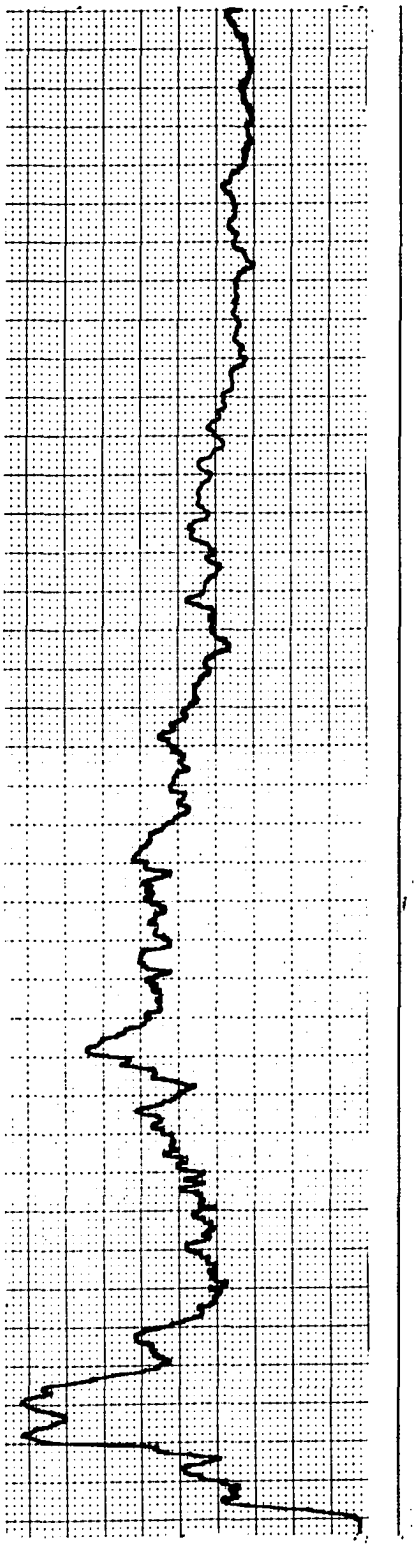

to be due to somewhat erratic sedimentation by groups of particles. It is now known to be a result of single particle attenuation which is in excess of the theoretical figure. This same effect, is efficiently utilized in single particle counting, which is described in detail in the next section.

To filter the above pulsations, a 500 microfarad capacitor was added across the photomultiplier output in parallel with the 2200 ohm load resistor, resulting in a response time of approximately one second. Evidently, while the individual particle effects were averaged, their total effect still resulted in too much attenuation at larger diameters. Particles with diameters below about five microns do not seem to cause excessive cavity attenuation. While there is a definite error involved from a theoretical standpoint, this error is consistent on tests made in any one size region and therefore can easily be calibrated out.

Figure 23 illustrates test results made on some talc powder. Note that agreement in this case is much better than that obtained on the larger diameter particles. Talc particles have irregular shapes which had to be converted to equivalent diameters for the microscopic tests. These equivalent diameters were those corresponding to the diameter of a circle with equal area. Note that while the laser output recording in Figure 28 is somewhat irregular, the data still converts very nicely to a reasonable size distribution curve.

Figure 24 is a comparison between microscopic and laser test data for S. S. White airbrasive powder. Agreement is less satisfactory than for talc particles but is still reasonable considering that these par-

ticles had irregular shapes also. Figure 27 shows the laser output recording for these particles. The narrow peak occurring during the first few seconds corresponds to the second peak in the microscopic curve in Figure 24. Due to the one second filter on the photomultiplier output, no quantitative photo-extinction data was obtained for these first few seconds. However, had the sedimentation chamber been substantially lengthened, a good quantitative record could have been taken, keeping in mind the offset error noticed on other previous tests.

It is somewhat difficult to correctly judge the results of the above photo-extinction work, due to the existence of excessive attenuation by larger particles. It is believed that good results can be obtained on photo-extinction tests made with the test laser on particles with diameters of near five microns or less. Above five microns, a correction is necessary to ensure satisfactory results. Since at least one microscopic analysis is necessary as a means of checking tests of this type, this does not present much of a problem because such a test could be used as a calibration. From the curves in Figures 21 and 22, it is apparent that a shift of 3-4 microns down to smaller diameters would give good results for a particle range of 5-30 microns. Since the method presented herein requires only very low test particle concentrations along with the ability to use photo-extinction with layered settling, the calibration effort does not seem excessive, compared to the advantages gained. However, for the 5-30 micron size region and higher, the new method of obtaining size frequency distributions presented in the next section appears to be superior in all respects. This is not nec-

essarily true for the less than five micron region and it is here that photo-extinction as described above presents a good approach to obtaining particle size distributions on an automated basis.

Single-Particle Detection

Introduction

There are several methods in existence today for detecting single particles with diameters in the micron region. All of these methods require very elaborate and expensive equipment. One approach is to detect the scattered light from a single particle. This requires a highly sensitive photomultiplier arrangement along with the necessity of reducing stray light to a minimum. Another approach is to have the particles mounted on a slide and use a microscope to focus the light to a very small spot. The spot is then automatically swept in a pattern across the slide with a photomultiplier detecting the changes in the transmitted light. Neither of these two methods are entirely satisfactory. The following method is presented as another approach to detecting single particles and determining particle size distributions. The experimental hardware for this method is illustrated in Figure 29.

Procedure

It is possible to utilize the error-causing effect of the photoextinction tests such that it itself can be used to determine particle size distributions. To do this it is necessary to switch from the concave-concave cavity configuration of the gas laser to the plane-concave geometry. This results in a cavity beam with a conical cross-section as illustrated in Figure 30. Note that the cross-section at the scattering chamber is much smaller than that at the spherical mirror surface. The size of the beam at the spherical mirror surface is very nearly that

Figure 29. Single-particle detection system

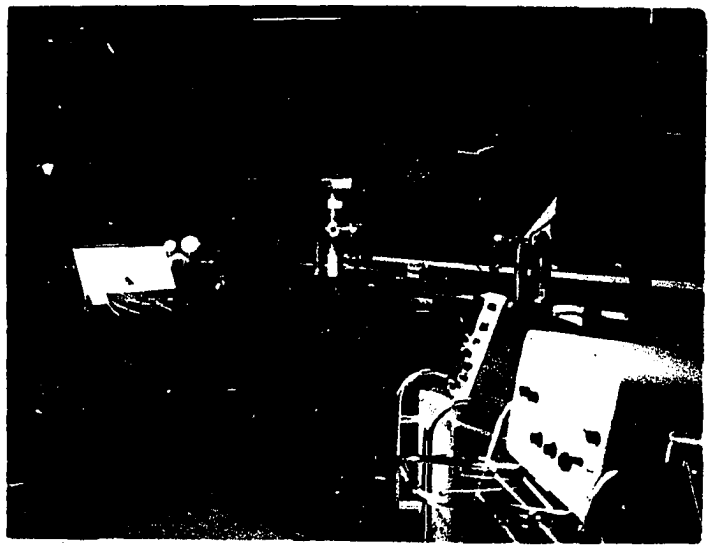

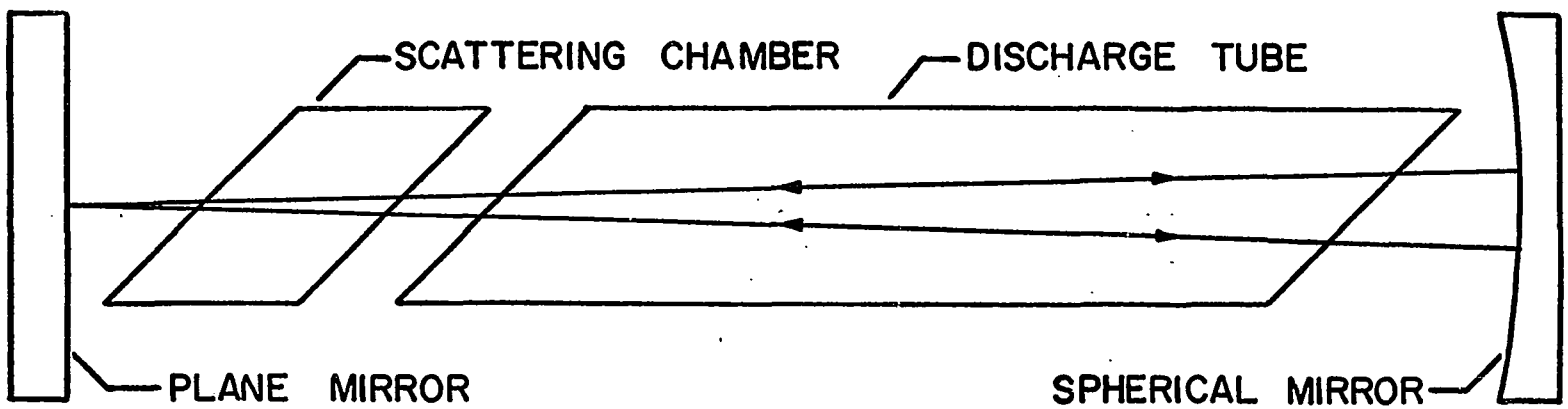

Figure 30. Ray geometry of the plane-concave cavity configuration

of the whole cavity when used in the concave-concave configuration. Therefore, it can be expected that the single-particle attenuation effect will be much greater when the plane mirror is used as one end of the cavity.

First, the filter capacitor across the photomultiplier output was removed to maximize single-particle detection sensitivity. Then, particles were again forced into the insertion chamber in the usual fashion after which the photomultiplier output was viewed on a scope. Cavity oscillation interruption was visible, as shown in Figure 31, and occurred for short periods of time. Note, that sometimes the output was only attenuated and not completely cutoff. It seemed, that erratic output of this type could only be caused by single particles entering the beam cross-section and interrupting oscillations.

To make sure that the observed effect was caused by single particles and not erratic particle group settling, a restricted cross-section was inserted into the settling chamber, thereby allowing very few particles to reach the beam. By observing the scope and settling chamber viewing port at the same time, it was firmly established that single particles were causing lasing oscillations to be completely quenched or severely attenuated.

Comparison of the particle cross-sectional areas with the beam cross-section in the scattering chamber does not explain the single-particle effect because the particle cross-section represents only a small portion of the beam cross-section. More likely, single-particle presence in the concentrated beam cross-section of the plane-concave

Figure 31. Gas laser in-cavity single-particle effects. Sweep speed of 5 sec/cm. Vertical sensitivity of 2 volts/cm.

Figure 32. Single-particle effects of a sedimentation run on 0-10 micron glass spheres. Sweep speed of 5 sec/cm. Vertical sensitivity of 2 volts/cm.

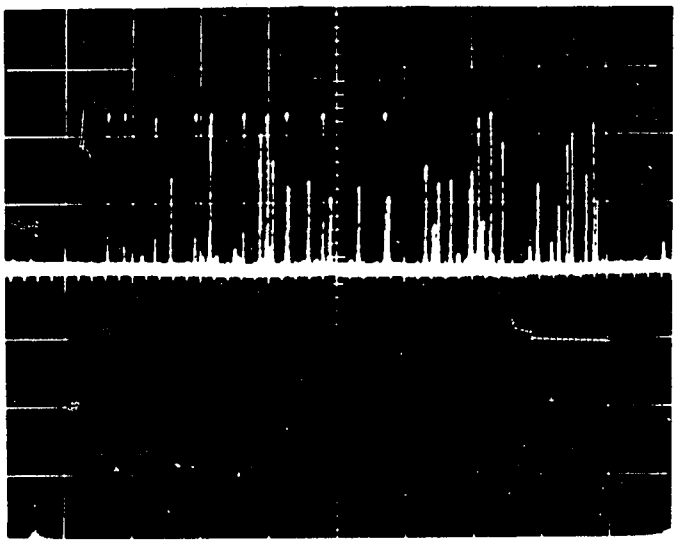

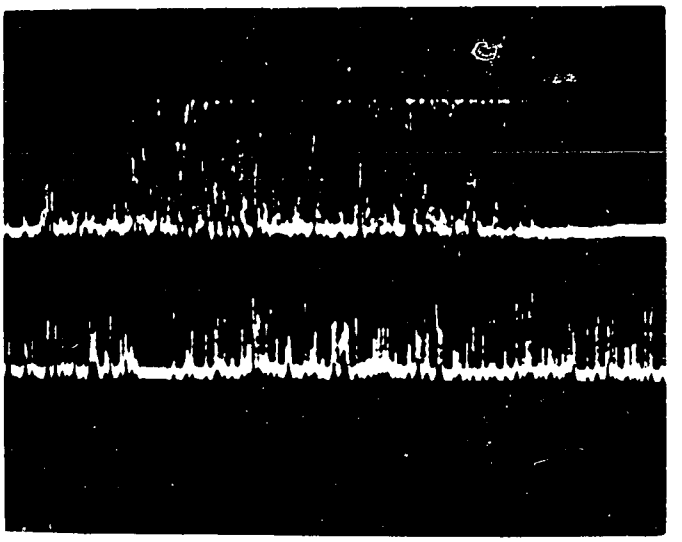

cavity geometry probably results in additional diffraction losses as determined by the unique properties of an oscillating cavity of this type. Analysis of the type done by Fox and Li (14) with the additional particle presence feature would help bring forth an explanation of the above phenomenon.

Since the plane-concave cavity geometry is so sensitive to single particle presence, as verified above, some work was initiated into the possibility of using this effect to determine particle size distributions. One way to accomplish this is to use layered sedimentation procedures with the laser cavity beam detecting the number of sedimenting particles passing per unit time. This is in contrast to turbidimetric sedimentation wherein the laser beam essentially measured the number of particles per unit volume which were present at any instant of time.

Analysis of Figure 31 indicated the possibility of using oscilloscope pictures as a particle versus time record. To get a particle size distribution curve from such data it is only necessary to determine the number of particles, m, that have passed the beam between any two times t_1 and t_2. Using equation 63, which was derived on page 54,

$$d = 10^4 \left(\frac{20.995}{3(10^5)\rho t} \right)^{\frac{1}{2}} \qquad 63$$

associated values of d_1 and d_2 corresponding to times t_1 and t_2 can be calculated. Equation 63 corresponds to the same sedimentation geometry as used before. Then,

$$d_1 - d_2 = \text{particle diameter span} \qquad 64$$

$$\frac{m}{d_1 - d_2} = \text{particles per micron} \qquad 65$$

Equations 64 and 65 result in a figure representing relative number of particles per micron size difference. Plotting equation 65 versus d_3 as given by

$$d_3 = d_1 + \frac{d_1 - d_2}{2} \qquad 66$$

and repeating this procedure for other times and diameters results in a size frequency versus diameter curve. Figure 33 is the resulting size frequency versus diameter curve obtained from a visual count of the oscilloscope photograph, Figure 32. Note the close correlation between the two curves, the other having been constructed through data obtained by a microscopic count. The abrupt ending of the laser-derived curve is a result of the upper trace ending at a time of 60 seconds. The bottom trace some time later.

Counting particles as evidenced on a photograph such as in Figure 32 is obviously a tedious job. Even so, it is much faster and more desirable than microscopic work in this respect. However, putting an electronic counter on the photomultiplier output resolves this problem in that, at least in principle, it is now possible to record the count versus time as the experiment progresses. Therefore, the remainder of the single-particle tests conducted herein were accomplished with an electronic counter doing the counting. There is the problem that an output count indication only exists until another particle is registered, leading to some difficulty in visually catching the exact count at a particular time. As will be seen later on, this does give rise to some erratic values but

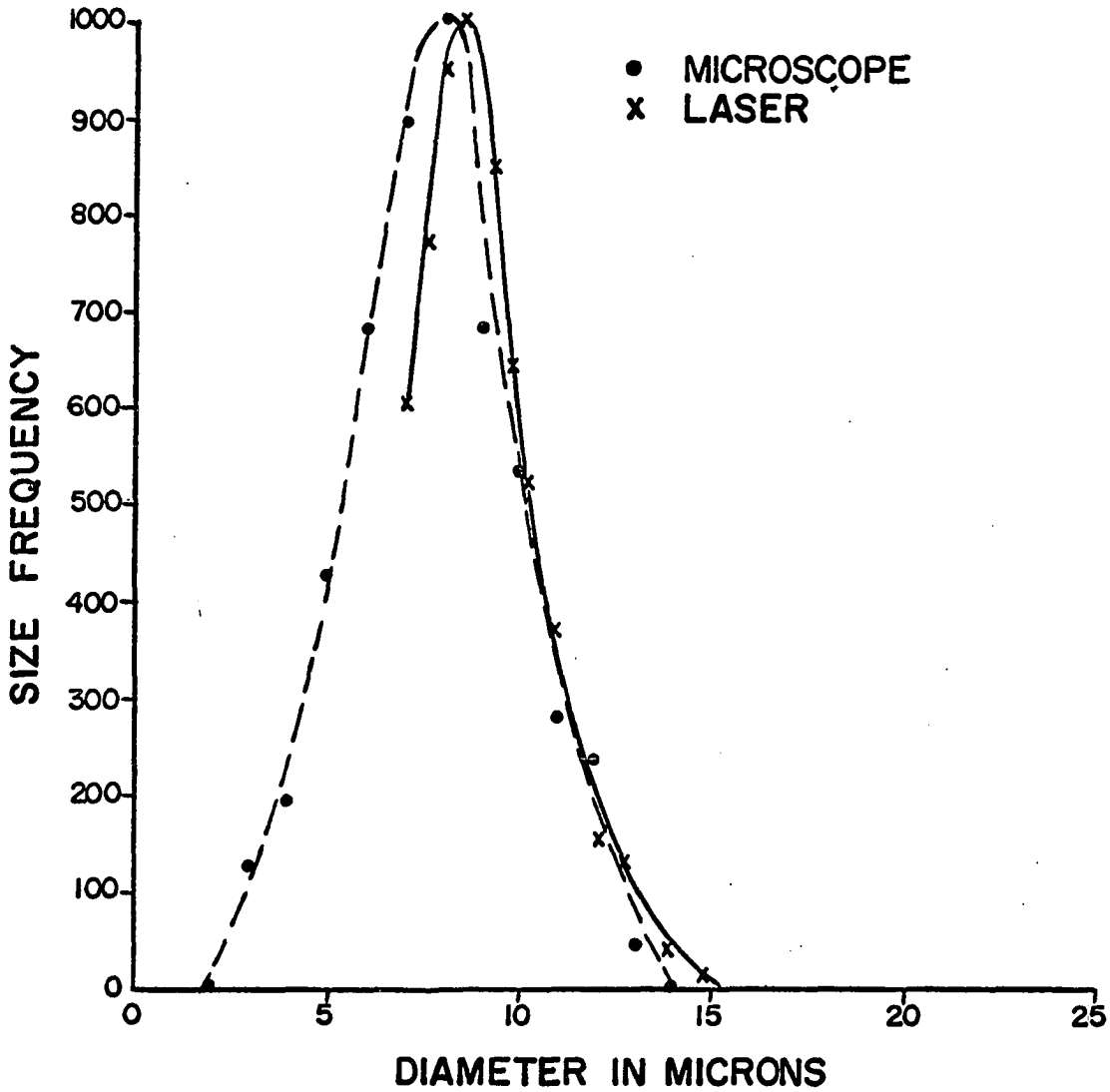

Figure 33. Particle size distribution of 0-10 micron glass spheres obtained by visual count method of Figure 32

in general does not appreciably affect the overall resulting curve. It seems possible that the count recording step can be readily automated.

Advantages

Advantages of using single-particle counting as compared with photo-extinction are the following:

A. No scattering coefficient effect
B. No loss calibration necessary
C. Easier data conversion to size distributions
D. Uses fewer particles
E. Can be used on absorbing particles
F. Insensitivity to detector placement

Elimination of the scattering coefficient from any consideration is highly desirable in that it is rarely known for other than spherical particles. Not having to measure losses eliminates the troublesome aspect of having to make relative energy measurements. The go no-go characteristic of single-particle recording is much simpler than any relative energy recording method. This go no-go characteristic also eliminates the calibration work necessary in photo-extinction measurements caused by the variation in laser gain with losses. Therefore, data-handling in single-particle detection work consists of simply counting with respect to time, followed by using equations 63 through 66.

While the low-loss photo-extinction method described before uses very few particles compared to normal photo-extinction methods, the single-particle counting approach uses even fewer. The low-loss photo-extinction method requires a density of about 5000 particles per cubic centimeter in the insertion chamber while the single-particle counting approach only needs about 200 per cubic centimeter. This represents a

factor of about 25 times fewer particles. Compared to normal photo-extinction densities of from 10^5 to 10^6 particles per cubic centimeter, single-particle counting uses about 2500 times fewer particles. This is a considerable reduction in particle density requirements and it is not known just how important this may be for present and future applications.

What could be the most important advantage, however, is the potential use on absorbing type particles. The photo-extinction method is sensitive to absorbing losses in addition to its scattering loss dependence. Therefore, photo-extinction is not too applicable to testing particles which do absorb at the wavelength involved. However, the single-particle counting method is largely impervious to absorption effects. In fact, absorption would only act to increase the system sensitivity, thereby making the system more useful.

The amount of light received by the detector in photo-extinction work depends both on the transmitted and scattered light due to large scattering effects in the small forward angles. Therefore, the solid angle subtended by the detector plays a very important part in using the photo-extinction method. Here again, the single-particle count method does not have such a difficulty in that its detector placement need only be such that most of the output signal variation is captured.

Disadvantages

There are only two areas wherein the photo-extinction method appears to have advantages over single-particle counting. One is the aforementioned problem of getting the electromic counter count inbetween counts.

Photo-extinction presents a nice continuous record with no comparable problem. The second area consists of the problem in getting a count when the particle size has been reduced to the point where low settling velocities are encountered. For a specific density of 2.5, this point occurs with particle sizes of about four microns. Not only is there difficulty in getting the counter to count correctly; but also, at these low settling velocities, there tends to be more than one particle in the beam at one time.

There are two difficulties characteristic of the single-particle counting method only. The first is the problem of recording enough counts for large particle settling. As mentioned before, Table 2 on page 63, shows the arrival and departure times of particles at the beam. It is clear that five seconds time difference in the 20-30 micron region encompasses many more microns size difference than in the 5-15 micron region. Therefore, for comparable accuracy, more counts should be recorded for these larger particles. Unfortunately, this is not too easily done. Fortunately, however, this whole problem can be circumvented by simply increasing the sedimentation distance to the beam, thereby resulting in more time per micron diameter change.

The second area of difficulty would seem to be associated with the beam edges. It is apparent from Figure 32 that some particles cause cutoff while others of the same size do not. It may be assumed that the cause is due to particle position in the beam varying from the beam edge to the beam center. This does not mean that part of the particle is in the beam while part of the particle is not. Rather, it indicates that

beam interruption near the outer portion does not entirely quench oscillations. This may be explained by the fact that the intensity of the beam across its cross-section varies in an approximately Gaussian manner. Since the counter must have a certain threshold level, smaller particles within the beam edge might not initiate a count while a larger particle might. Therefore, this effect would tend to shift the size frequency curve towards larger diameters. At the same time, smaller particles tend to linger in the beam longer and are more apt to initiate a multiple count thereby tending to neutralize the edge effect. In either case, both effects are probably within the experimental errors incurred from other causes.

Results

Figure 34 represents a comparison between the single-particle count method and a microscopic size check for 0-10 micron glass spheres. Note the excellent agreement between the two methods. The somewhat erratic spacing of the individual points is probably due to both visual count recording difficulties and possible dispersion irregularities. Figure 35 is a comparison between the two methods for 10-20 micron glass spheres. Again note the close agreement, although the experimental point at twenty microns is debatable. That this point might not compare very well is not too surprising since in the twenty micron region, a five second interval between readings encompasses almost seven microns over which the count must be averaged. To get a better representation of the upper side of this curve, it is only necessary to increase the sedimentation distance as discussed before.

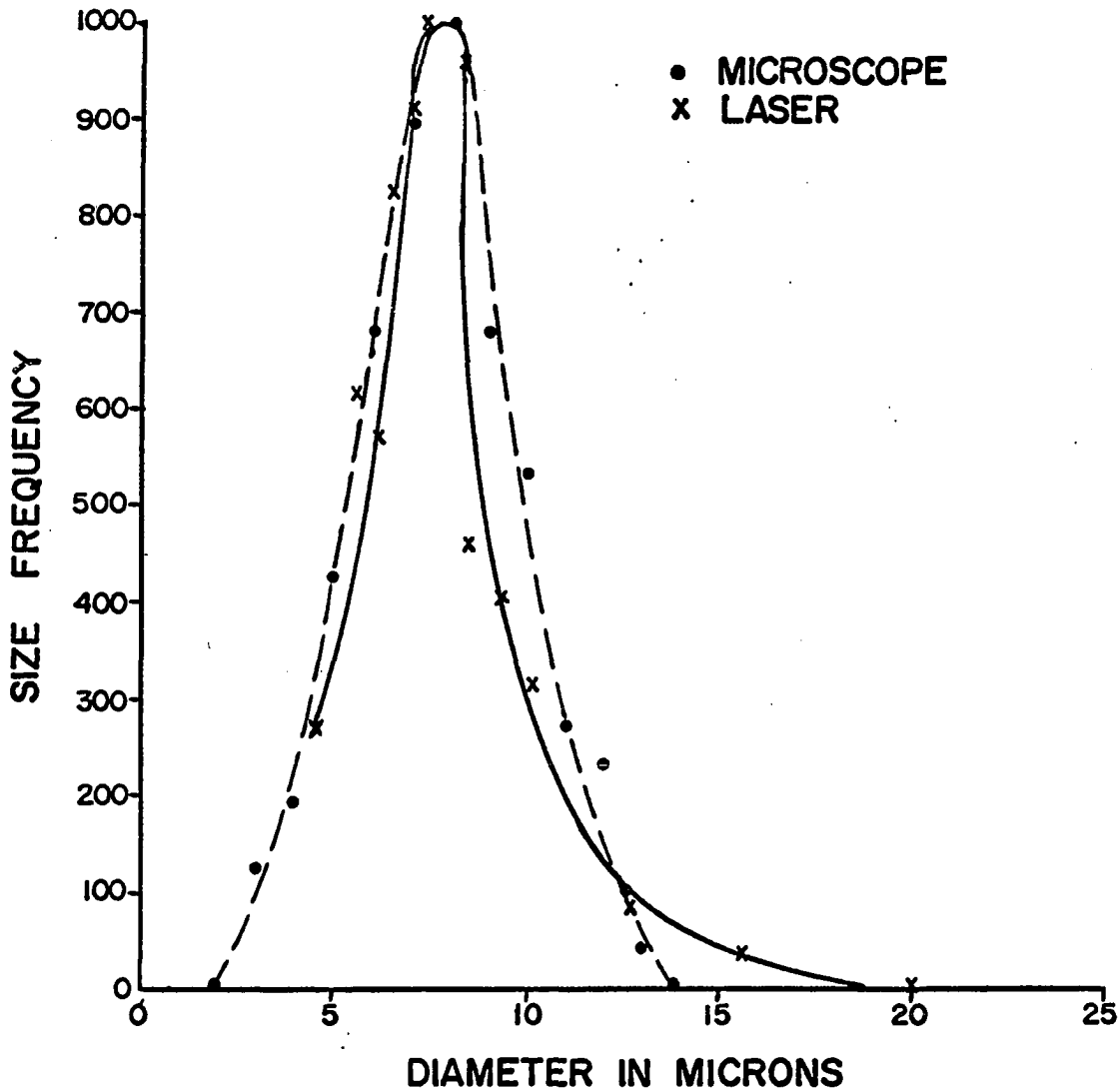

Figure 34. Single-particle count method size distribution results for 0-10 micron glass spheres

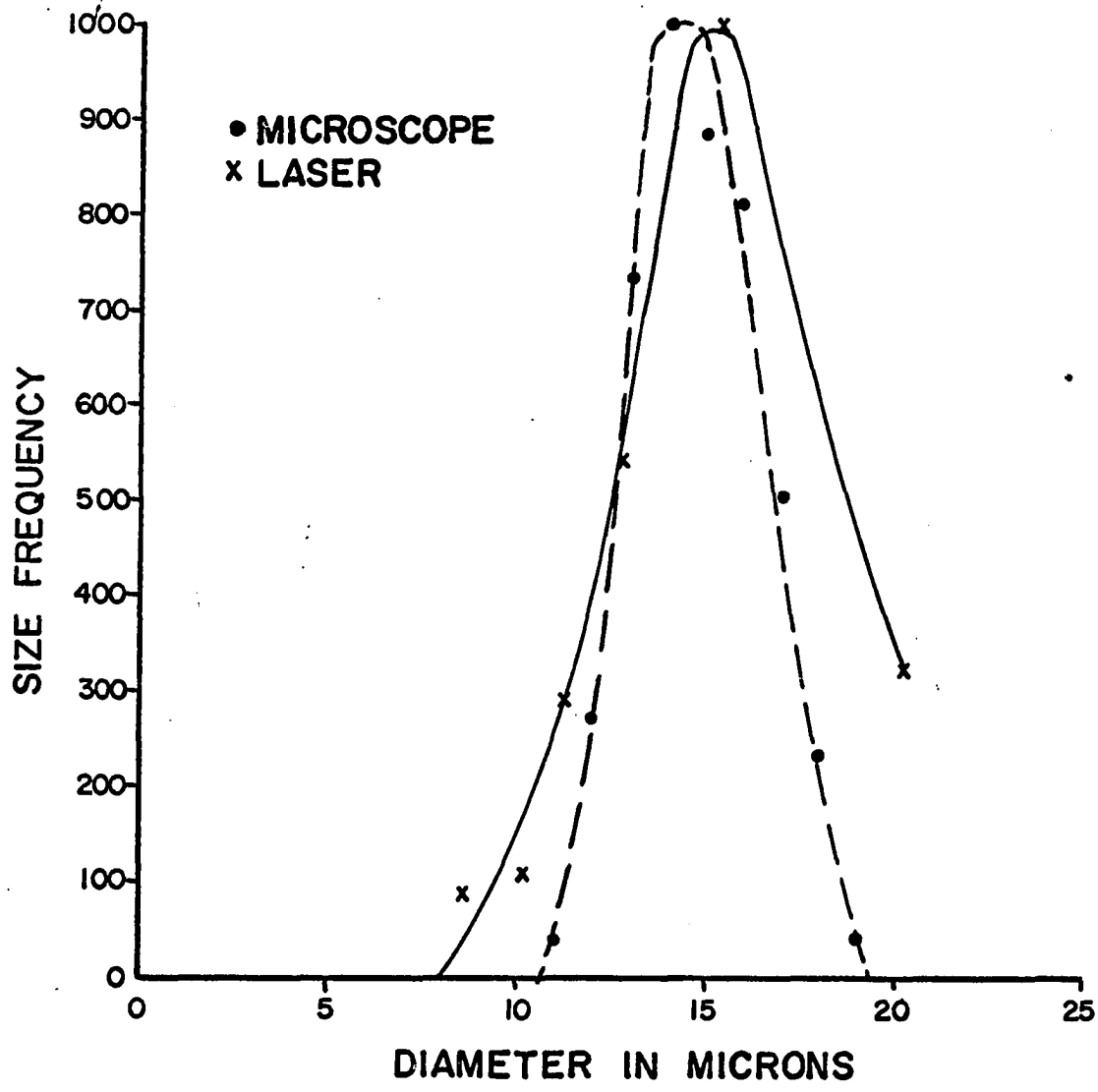

Figure 35. Single-particle count method size distribution results for 10-20 micron glass spheres

To check the single-particle count method on irregularly shaped particles, both talc and S. S. White airbrasive powder were again tested. The particle size analysis of talc is compared with microscopic measurements in Figure 36. As in the photo-extinction work, the microscopic diameters are those corresponding to the diameter of a circle with equal area. Agreement seems to be fair and any observed discrepancy can be easily attributed to diameter definition for irregularly shaped particles. Figure 37 indicates somewhat closer agreement for the airbrasive powder. Here again, the particles are irregularly shaped, although not to the extent that talc particles are.

It was noticed that during single-particle counting runs on irregularly shaped particles, the electronic counter indicated very erratic counting for particles of a size near three microns or less. The cause of this was subsequently determined to be due to the rotating motion of an irregularly shaped particle as it crossed the beam. These rotating particles evidently provide a varying cross-section in the beam, thereby varying the output with each rotation to an extent sufficient to trigger the counter at a very fast rate. An effort was made to catch a rotating particle in the beam with a faster scope sweep such that its rotation frequency could be obtained. Figure 38 shows multiple sweeps at a speed of 0.1 second per centimeter and a vertical sensitivity of 2 volts per centimeter. This picture was taken about 4 minutes and 45 seconds after insertion of S. S. White airbrasive powder. Note the two traces due to a particle in the beam rotating with an apparent angular frequency of 45 revolutions per second. Since these particles have

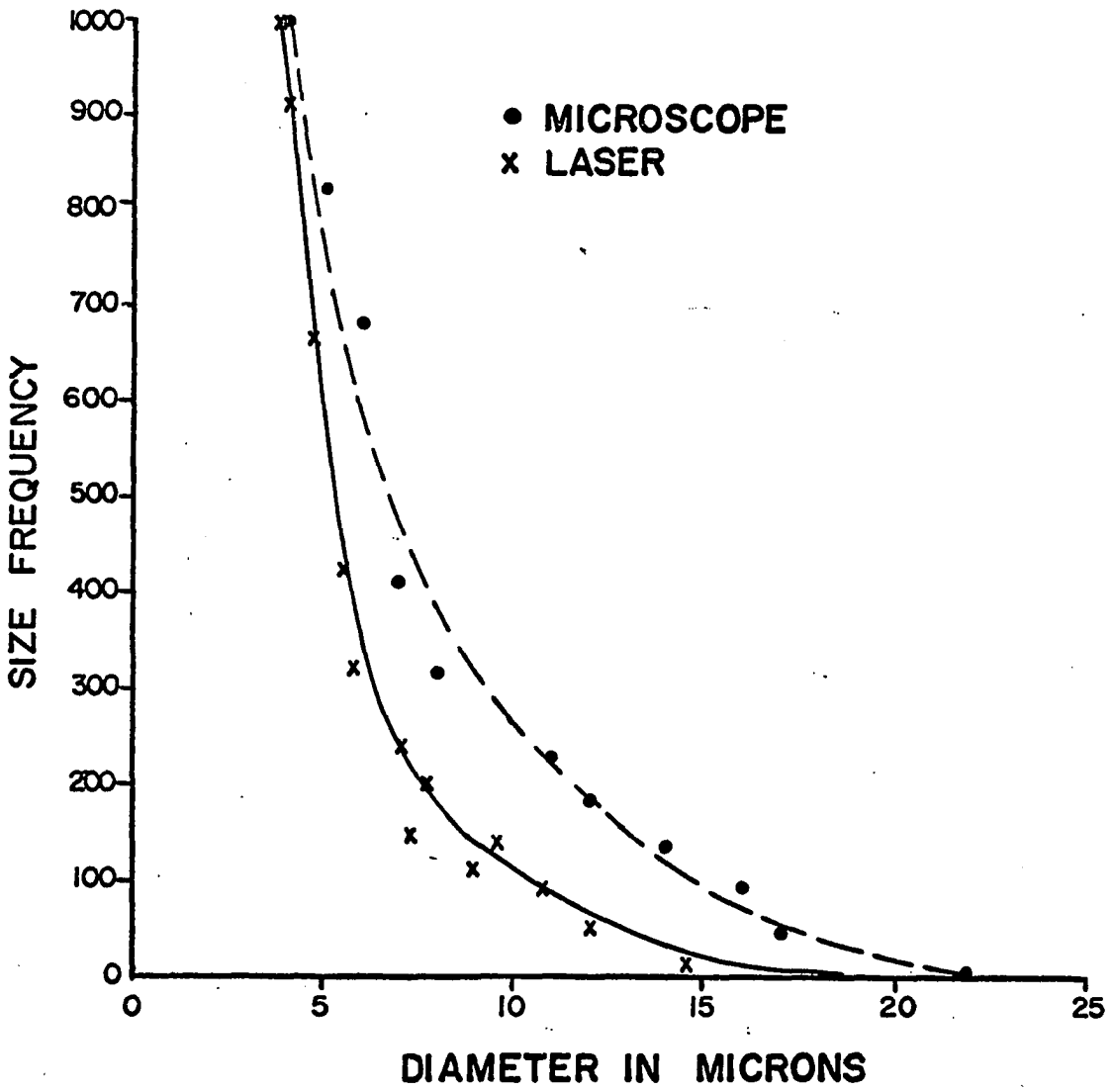

Figure 36. Single-particle count method size distribution results for talc particles

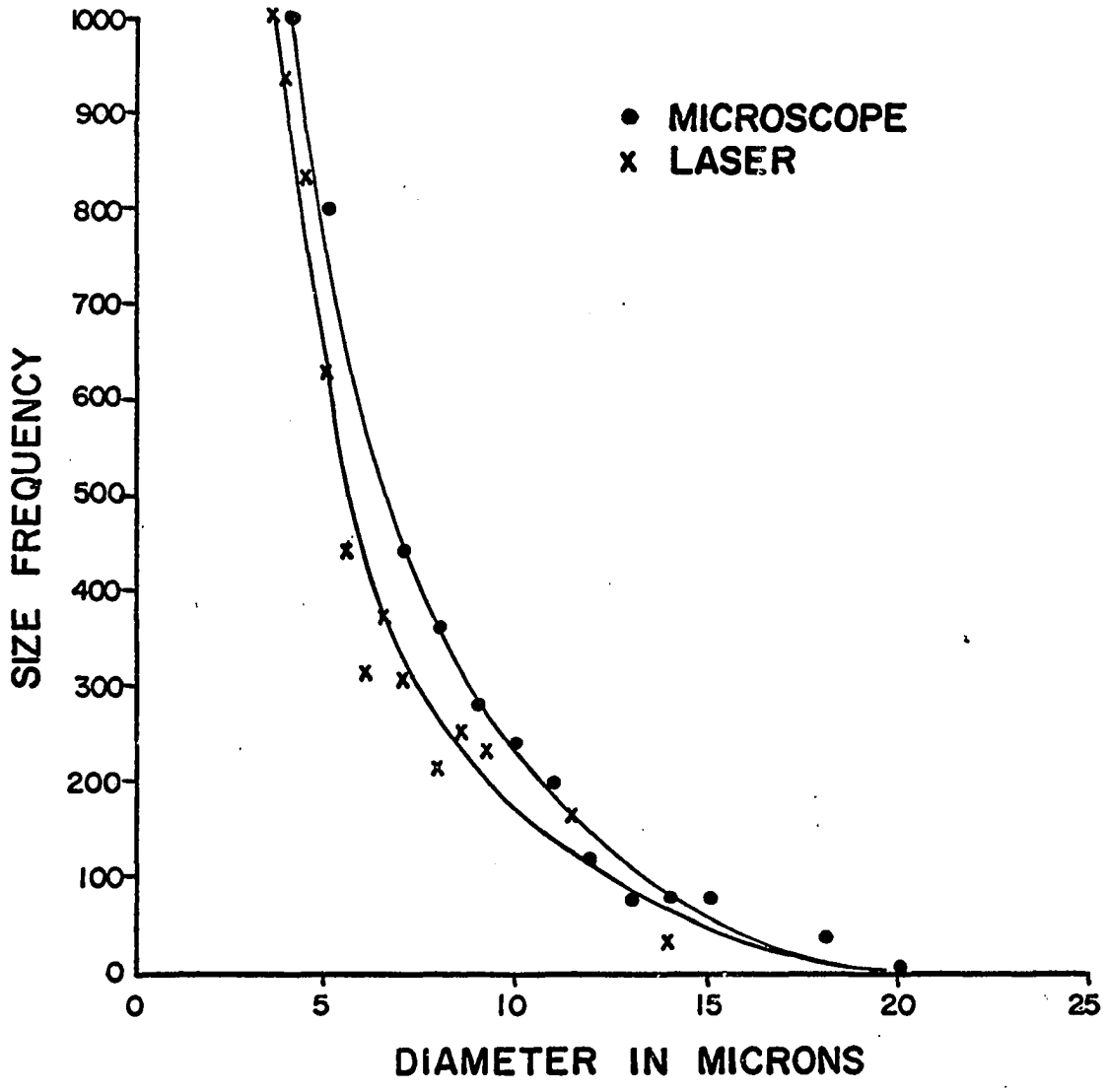

Figure 37. Single-particle count method size distribution results for S. S. White airbrasive particles

Figure 38. Single-particle rotational effects of a 2-3 micron irregularly shaped S. S. White airbrasive particle. Sweep speed of 0.1 sec/cm. Vertical sensitivity of 2 volts/cm.

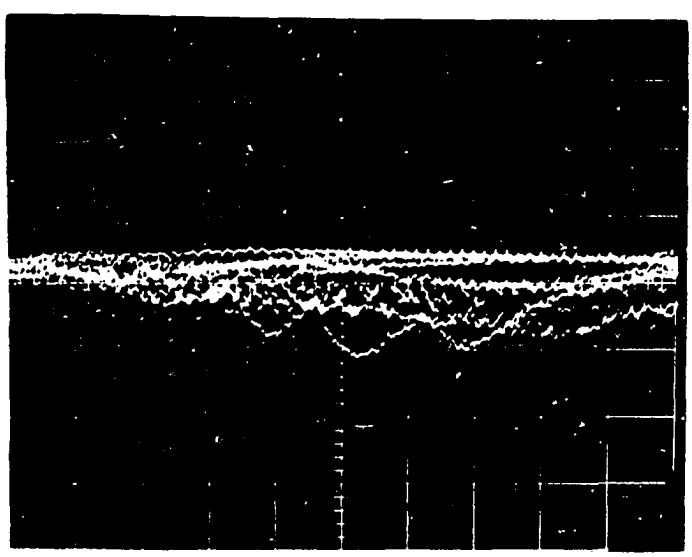

irregular shapes, the actual rotating frequency could be less if a peculiar shape were involved. The other traces either show that no particle is present at the sweep time or that a particle is present but not spinning. Figure 38 certainly gives an indication of the high sensitivity of this system and there may be some interesting applications in this area.

The single-particle counting method seems to be a quite useful tool for determining particle size distributions for particles with diameters above three microns. Extending the cavity length to two or three meters would tend to further reduce the beam cross-section and perhaps extend the lower limit to less than three microns. The upper size limit depends on Stokes' law validity for settling in air and would therefore fall near the fifty micron size. Within its size range, it is doubtful that any other sedimentation method can be found that will even approach the low particle concentrations that can be used in single-particle counting. Further work in the count recording area is desirable and any improvement here would increase its accuracy.

SUMMARY

This dissertation has been concerned with light absorption, refraction, and scattering in in-cavity experiments utilizing a 6328 angstrom helium-neon gas laser. The primary motivation was to discover new applications in which gas lasers could make significant contributions. To this end, experiments were run concerning index of refraction changes, low vapor pressure absorption, and small particle scattering.

The index of refraction test results showed that if the test medium can be inserted into the laser cavity, then index of refraction changes can be detected with a sensitivity higher than that from light beam bending alone. The extra sensitivity is provided by the cavity misalignment that occurs with test medium index of refraction changes. The combination of cavity misalignment and transverse beam bending results in a sensitivity of about 15 millivolts per millimeter of mercury change. The time response of this type of index of refraction measurement is limited by the photomultiplier detector only, and this can be made to respond in the nanosecond region. Possible applications include shock tubes, wind tunnels, and any other situation where a fast index of refraction change is involved.

To measure very low light losses within the laser cavity it is necessary to have a means of calibrating such losses. This was solved by inserting a very thin optical flat into one end of the laser cavity with the test cell in the other. Then, by varying the angle of the thin flat until the laser output coincided with that measured during the test, it is possible to determine the loss associated with the test. System

sensitivity of one-hundredth of a percent and a measuring range of one percent are achieved. Possible applications of such a low-light-loss measuring device occur in low vapor pressure absorption studies and small particle scattering.

To test the feasibility of using the gas laser in the above manner, a short absorption cell was constructed into which a small crystal of iodine was placed. The resulting absorption loss compared very well with that published in the literature. Turbidimetric sedimentation tests utilizing layered settling techniques were also completed. These test results indicate that some calibration is necessary for particles larger than five microns. Good theoretical agreement can be expected below five microns. Particle concentrations for these tests were only about 5000 particles per cubic centimeter.

When the gas laser is placed in its plane-concave configuration, laser oscillations can be completely quenched by small particle presence in the beam near the plane mirror. This phenomenon can be effectively used to measure particle size distributions by using layered sedimentation techniques. This approach to particle size measurement is quite simple and uses extremely low particle concentrations. The combination of low particle concentration, simple measuring technique, and easy data conversion certainly makes this a method worthy of further investigation and use.

From the above results, it is clear that the low-light-loss sensitivity of a gas laser cavity, together with the calibration ability of the variable Brewster-angle flat, can be used to measure very low light

losses that would otherwise not be detectable. This, in conjunction with the newly developed single-particle counting size distribution method, certainly places the 6328 angstrom gas laser in the category of useful instruments.

LITERATURE CITED

1. Schawlow, A. L. and Townes, C. H. Infrared and optical masers. Physical Review 112: 1940-1949. 1958.

2. Maiman, T. H. Stimulated optical radiation in ruby. Nature 187: 493-494. 1960.

3. Javan, A. Possibility of production of negative temperature in gas discharges. Physical Review Letters 3: 87. 1959.

4. Bennett, W. R. Gaseous optical masers. Applied Optics Supplement No. 1 on Optical Masers 24-61. 1962.

5. Born, M. and Wolf, E. Principles of optics. New York, N. Y., Pergamon Press, Inc. 1959.

6. Lothian, G. F. Absorption spectrophotometry. 2nd ed. New York, N. Y., The Macmillan Co. 1958.

7. Goy, C. A. and Pritchard, H. O. Pressure dependence of the visible iodine band. Journal of Molecular Spectroscopy 12: 38-44. 1964.

8. Cadle, R. D. Particle size determination. New York, N. Y., Interscience Publishers, Inc. 1955.

9. Sinclair, D. Stability of aerosols and behavior of aerosol particles. U. S. Atomic Energy Comm. Handbook on Aerosols. 64-76. 1950.

10. Irani, R. R. and Callis, C. F. Particle size: measurement, interpretation, and application. New York, N. Y., John Wiley and Sons, Inc. 1963.

11. Rose, H. E. The measurement of particle size in very fine powders. London, England, Constable and Company, Ltd. 1953.

12. Marshall, C. E. A new method of determining the distribution curve of polydisperse colloidal systems. Proceedings Royal Society of London 126: 427-430. 1930.

13. Dallavalle, J. M. Micromeritics: the technology of fine particles. 2nd ed. New York, N. Y., Pitman Publishing Corp. 1948.

14. Fox, A. G. and Li. Tingye. Resonant modes in a maser interferometer. Bell System Technical Journal 40: 453-488. 1961.

ACKNOWLEDGEMENTS

The author of this dissertation gratefully acknowledges the complete freedom accorded by his major professor, Dr. A. A. Read, in choosing the research area contained herein.

The author is also indebted to Ed DeKalb, Richard Kniseley, and Dr. A. J. Bureau for their help in locating experimental equipment. Deep appreciation is also felt for the support received from the National Defense Fellowship which has made his graduate program possible. Full acknowledgement of the financial aid for summer employment by the National Science Foundation Thin-Film Grant at Iowa State University is also in order.